



1

**CROSSING CHARACTERISTICS OF WEB GIRDERS IN  
UNIDIRECTIONALLY STIFFENED DOUBLE HULL STRUCTURES**

by

**JENNIFER CULBERTSON DRISCOLL**  
B.S. Naval Architecture, United States Naval Academy (1987)

**SUBMITTED TO THE DEPARTMENT OF  
OCEAN ENGINEERING**

**IN PARTIAL FULFILLMENT OF THE REQUIREMENTS**

**FOR THE DEGREES OF**

**MASTER OF SCIENCE IN NAVAL ARCHITECTURE AND MARINE ENGINEERING**

and

**MASTER OF SCIENCE IN MECHANICAL ENGINEERING**

at the

**MASSACHUSETTS INSTITUTE OF TECHNOLOGY**  
June, 1992

**DTIC**  
**ELECTE**  
SEP 1 1992  
**S**  
**C**  
**D**

© Jennifer Culbertson Driscoll, 1992. All rights reserved.

The author hereby grants to MIT and the U.S. Government  
permission to reproduce and to distribute copies of  
this thesis document in whole or in part.

Signature of Author..... *Jennifer Culbertson Driscoll*.....  
Department of Ocean Engineering  
May, 1992

Certified by..... *Tomasz Nierzwicki*.....  
*Tomasz Nierzwicki*  
Thesis Supervisor

Certified by..... *David M Parks*.....  
*David M Parks*  
D. M. Parks  
Thesis Reader

Accepted by..... *A. Douglas Carmichael*.....  
*A. Douglas Carmichael*, Chairman  
Department Committee on Graduate Studies  
Department of Ocean Engineering

Approved for release  
Distribution Unlimited

92 8 31 010

406854  
92-24093  
83P



CRUSHING CHARACTERISTICS OF WEB GIRDERS IN  
UNIDIRECTIONALLY STIFFENED DOUBLE HULL STRUCTURES

by

JENNIFER CULBERTSON DRISCOLL  
B.S. Naval Architecture, U. S. Naval Academy (1987)

Submitted to the Department of Ocean Engineering in partial fulfillment of the requirements for the degrees of Master of Science in Naval Architecture and Marine Engineering and Master of Science in Mechanical Engineering

ABSTRACT

This paper examines the crushing characteristics of a web girder subjected to a local in-plane crushing load. First, a simplified model of the post-buckling deformation of the web girder is developed. Then this model is used to formulate an upper-bound solution for the plastic behavior of the deforming web girder. Finally small-scale crushing tests of extruded aluminum double-hollow forms are conducted to verify the deformation mode and the upper-bound solution. The web girders of interest for this research are the longitudinal web girders in a unidirectionally stiffened double hull (USDH) structure.

DTIC QUALITY INSPECTED 3

Accession For	
NTIS Grant	<input checked="" type="checkbox"/>
DTIC Ref	<input type="checkbox"/>
Unannounced	<input type="checkbox"/>
Justification	
Rec Form 50	
Distribution/	
Availability Codes	
Dist	Avail and/or Special
A-1	

## TABLE OF CONTENTS

1.	INTRODUCTION . . . . .	5
2.	PROBLEM DEFINITION . . . . .	9
	2.1. UPPER BOUND THEOREM APPROACH . . . . .	9
	2.2. STRUCTURAL UNIT . . . . .	10
	2.3. LOADING CONDITION . . . . .	10
	2.4. MATERIAL PROPERTIES . . . . .	11
	2.5. LIST OF NOMENCLATURE . . . . .	12
3.	LOCAL DENTING MODE . . . . .	14
	3.1. SIMPLIFIED MODEL . . . . .	14
	3.2. DEFORMATION SEQUENCE . . . . .	15
	3.3. LOAD-DEFLECTION RELATIONSHIP . . . . .	15
	3.3.1.    RATE OF INTERNAL ENERGY DISSIPATION . . . . .	16
	3.3.1.1.    BENDING ENERGY RATE . . . . .	16
	3.3.1.2.    MEMBRANE ENERGY RATE . . . . .	20
	3.3.2.    RATE OF EXTERNAL WORK . . . . .	23
	3.3.3.    PHYSICAL LIMIT . . . . .	24
	3.3.4.    INITIAL PHASE ENVELOPE . . . . .	25
	3.3.5.    STRAIN HARDENING . . . . .	26
4.	GLOBAL BENDING MODE . . . . .	28
	4.1. SIMPLIFIED MODEL . . . . .	28
	4.2. DEFORMATION SEQUENCE . . . . .	28
	4.3. LOAD-DEFLECTION RELATIONSHIP . . . . .	29
	4.3.1.    RATE OF INTERNAL ENERGY DISSIPATION . . . . .	30
	4.3.1.1.    BENDING ENERGY RATE . . . . .	31
	4.3.1.2.    MEMBRANE ENERGY RATE . . . . .	33
	4.3.1.3.    SECONDARY MECHANISMS . . . . .	33
	4.3.2.    RATE OF EXTERNAL WORK . . . . .	34
	4.3.3.    PHYSICAL LIMIT . . . . .	35
	4.3.4.    GLOBAL LOAD-DEFLECTION RELATIONSHIP . . . . .	36
	4.3.5.    STRAIN HARDENING . . . . .	38
	4.4. COMBINED DENTING-BENDING MODEL . . . . .	38

TABLE OF CONTENTS, CONT'D

5. CRUSHING EXPERIMENTS . . . . . 39

5.1. BACKGROUND . . . . . 39

5.2. LOCAL DENTING . . . . . 40

5.2.1. DESCRIPTION OF DEFORMATION . . . . . 41

5.2.2. LOAD-DEFLECTION CURVES . . . . . 41

5.3. GLOBAL BENDING . . . . . 42

5.3.1. DESCRIPTION OF DEFORMATION . . . . . 43

5.3.2. LOAD DEFLECTION CURVES . . . . . 43

6. CONCLUSIONS & RECOMMENDATIONS . . . . . 45

REFERENCES . . . . . 49

BIBLIOGRAPHY . . . . . 51

APPENDIX A: LOCAL DENTING MODEL . . . . . 52

APPENDIX B: GLOBAL BENDING MODEL . . . . . 55

APPENDIX C: CRUSHING EXPERIMENT SET-UP . . . . . 59

APPENDIX D: EXPERIMENT SPECIMEN SPECIFICATIONS . . . . . 60

FIGURES . . . . . 62

## 1. INTRODUCTION

The ability of ships to withstand damage--whether from collision, grounding, or explosion--is an active concern of naval architects and ship owners. In 1985, the Hitachi Zosen Corporation of Japan presented the concept of an advanced double hull design which utilizes longitudinal girders connecting inner and outer hulls to form a cellular structure that wraps around the girth of a hull.<sup>[1]</sup> Among other advantages, this unidirectionally stiffened double hull (USDH) structure, shown in Figure 1, offers the potential of increased protection against local damage resulting from accidental loading. This potential has contributed to recent interest in the USDH structure for both commercial and naval ship designs.<sup>[2]</sup>

Damage to ships involves a complex interaction of structural members. While several authors have developed models of ship collisions, research concerning ship groundings is in the initial stages. Most ship damage models have dealt with conventionally framed ships which utilize a gridwork system of large transverse web frames intersected by smaller longitudinal stiffeners. In general, for both collisions and groundings, these transverse web frames are subjected to large compressive in-plane loads.

McDermott et al.<sup>[3]</sup> developed a mathematical model of the various stages involved in a minor collision of longitudinally framed oil tankers. This model was applied to both single hull

and double hull tankers. McDermott assumed that the resistance offered by a buckled web frame remained constant during deformation of the web frame in the transverse direction. Chang<sup>(4)</sup> in his discussion of McDermott's paper recommended that the post-buckling resistance of web frames be further investigated because many structural members offer decreased resistance after an ultimate strength has been reached.

Wierzbicki et al.<sup>(5)</sup> investigated the extent of damages involved in high energy groundings of tankers for a study conducted for the Joint M.I.T.-Industry Program on Safe Tankers. For this study, a simplified model was developed to predict the energy dissipated by the crushing of transverse web frames.

This model utilized the assumption that the deformation of the transverse web frame and the hull plating which acts as a flange could be separated into two mechanisms. It was assumed that the web detaches from the flange and rolls into two cylinders of equal radii, one on either side of the point of load application. It was assumed that the hull plating deforms into a trough shape. A sketch of this model is shown in Figure 2. Geometric compatibility of the connection between the web and the attached plating, however, was not maintained.

Instead of simplifying the post-failure resistance of deforming webs by modelling the resistance as a constant, the plastic behavior of the web may be described by a non-linear spring in a global model of a ship structure.

For example, the USDH structure can be considered to be a sandwich structure with a definable crushing strength of the core, a finite shear strength in the direction of the longitudinal web girders, and negligible shear strength in the transverse direction normal to the web girders. This sandwich structure can be modelled as rigid-plastic membranes (representing the inner and outer hull plating) connected by vertical (crushing strength) and diagonal (shear strength) non-linear springs.<sup>[6]</sup> This model is shown in Figure 3.

The objective of this study is to develop the load-deformation characteristics for longitudinal web girders subjected to local in-plane crushing loads. These characteristics can then be used to describe the vertical springs of the model described above.

The crushing of longitudinal web girders presents a problem similar to that of crushing tubular members. Several studies have been conducted which have explored the large deflection plastic behavior of thin walled tubular members. Reference [7] contains a review of several of these studies. Much of the analyses involving crushing of tubular members is focused on crushing due to axial loads. This class of problems lends itself to simple modelling due to the axi-symmetrical cross-section of tubular members.

The crushing of longitudinal girders in the USDH structure, however, is similar to crushing of tubes subjected to lateral loads rather than axial loads. De Oliveira et. al.<sup>[8]</sup> present

an analysis of crushing of circular tubes due to lateral loads. This class of problems is more difficult to analyze due to a lack of symmetry and due to the fact that a tube's cross-sectional shape changes during deformation. If the crushing load is localized rather than distributed, the distortion of the cross-sectional shape occurs locally and propagates. This propagation of damage is difficult to predict without experimental results.

The problem under consideration for this study resembles crushing of a multiple box column-type structure subjected to a localized lateral load. Although de Oliveira's work focused on crushing of circular tubes, the same approach of using simple methods of structural plasticity applied to a simplified deformation model is used for this study.

First, models for two modes of deformation of a web girder--local denting and global bending--are developed based on some photographic evidence of the deformation of fully clamped plates that were subjected to in-plane impact loading. Next, upper-bound solutions for the plastic behavior of deforming web girders are formulated for each mode. Finally, theoretical predictions based on the upper-bound solutions are compared to the results from a limited number of small-scale crushing experiments.

## 2. PROBLEM DEFINITION

2.1. UPPER-BOUND THEOREM: An upper-bound approach will be used to find the crushing characteristics of a web girder subjected to a local in-plane crushing load. Calladine <sup>[9]</sup> provides a concise statement of the Upper-bound Theorem:

"If an estimate of the plastic collapse load of a body is made by equating internal rate of dissipation of energy to the rate at which external forces do work in any postulated mechanism of deformation of the body, the estimate will be either high, or correct."

The postulated mechanisms of deformation to which Calladine refers to must be kinematically admissible.

Two modes of deformation are postulated for this study. The first mode involves local indentation of the web girder. The second mode involves the development of a three hinge mechanism to induce global bending of the web girder between transverse bulkheads. These postulated deformation mechanisms are described in sections 3 and 4. Assumptions concerning the geometry and boundary conditions of the deforming body, the material properties of the body and the applied external loads for this solution are described in the following sections.

**2.2. STRUCTURAL UNIT:** Figure 4 shows a section of the USDH structure consisting of rectangular cells. This cellular structure runs between transverse bulkheads and wraps around the girth of a hull. Due to symmetry it is sufficient to define a structural unit which consists of one longitudinal web girder with the attached inner and outer hull plating. This structural unit is shown in Figure 5.

The depth of the web girder is "H" and the thickness of the web girder is " $t_w$ ". Because the inner and outer hull plating act as fully effective flanges, the breadth of the attached plating is equal to the girder spacing, "B". The thickness of the hull plating is " $t_p$ ". The length of the web girder is determined by the distance between transverse bulkheads. This length is much greater than the girder depth and spacing. The structural unit, therefore, can be assumed to be effectively infinite in the longitudinal direction.

Due to symmetry, the attached hull plating flanges are constrained from in-plane movement in the X-direction along the longitudinal edges ( $X = \pm B/2$ ). Both ends of the structural unit are considered to be fully clamped at the transverse bulkheads ( $Y = \pm L/2$ ).

**2.3. LOADING CONDITION:** The web girder is considered to be subjected to a local crushing load such as that delivered by a knife-edge indenter or a rigid punch normal to the longitudinal axis of symmetry. This loading is quasi-static, therefore

dynamic effects are ignored. The applied load has a magnitude of  $P_0$ . This load causes the flange to deflect a distance  $\Delta$  relative to the un-deformed region of the flange. The rate of deflection is denoted by  $\dot{\Delta}$ .

**2.4. MATERIAL PROPERTIES AND ASSUMPTIONS:** The material is assumed to be rigid/plastic isotropic time-independent material which can be described by the flow stress  $\sigma_0$ . Strain hardening effects may be included by adjusting the value of the flow stress based on the average plastic strains of the deforming regions during the deformation process. The average plastic strain may be obtained by integrating the strain over the length of the deforming region:

$$\epsilon_{avg} = \frac{1}{L} \int_0^L \epsilon(z) dz \quad . \quad (1)$$

Bending stresses and membrane stresses are modelled as uncoupled. Deforming regions which experience high bending stresses are considered to have negligible membrane stresses. Likewise, regions which develop significant membrane stresses are assumed to have negligible bending stresses.

2.5. LIST OF NOMENCLATURE: This section provides a list of the symbols and parameters used in this paper.

HULL PARAMETERS

H: Depth of web;  
B: Longitudinal girder spacing;  
 $t_w$ : Thickness of web;  
 $t_p$ : Thickness of inner and outer hull plating  
L: Distance between transverse bulkheads;  
 $H^*$ :  $H / t_w$ ;  
 $B^*$ :  $B / t_p$ ;  
 $t^*$ :  $t_p / t_w$ ;  
 $L^*$ :  $L / H$ ;

MATERIAL PARAMETERS

$\sigma_o$ : Flow stress;  
 $\sigma_{ult}$ : Ultimate tensile yield stress;  
 $\epsilon_{ult}$ : Ultimate tensile strain;  
 $M_o$ : Fully plastic bending moment for the web;  
 $\bar{M}_o$ : Fully plastic bending moment for the flanges;  
 $M_u$ :  $(\sigma_u t_w^2) / 4$   
 $N_o$ : Fully plastic membrane force for the web;  
 $\bar{N}_o$ : Fully plastic membrane force for the flanges;

GEOMETRIC PARAMETERS

$\Delta$ : Crushing depth;  
 $\Delta^*$ :  $\Delta / H$ ;  
 $\delta$ : Local crushing depth for global bending mode;  
 $\zeta$ : Vertical extent of damage for local denting mode;  
 $\zeta^*$ :  $\zeta / H$ ;  
 $\alpha$ : Angle between first and second hinge lines;  
 $\beta$ : Angle between second and third hinge lines;

## GEOMETRIC PARAMETERS, CONTINUED

$\theta_o$ :	Angle of indentation due to crushing;
$\theta_i$ :	Angle between regions connected to the i'th hinge line;
$l_i$ :	Length of i'th hinge line;
$\Phi$ :	Angle between the first and third hinge lines;
$\phi$ :	Angle between center line and third hinge line;
$\gamma$ :	Angle of depression in global bending mode;
$u_f$ :	Stretching of flange;
$u_x$ :	Maximum stretching of web;
$\epsilon_f$ :	Average strain for flange;
$\epsilon_x$ :	Maximum strain for web;
$\epsilon_{avg}$ :	Average strain for structural unit;
$P_B$ :	Crushing force.

### 3. LOCAL DENTING MODE

**3.1. SIMPLIFIED MODEL:** Figure 6 shows a photograph of a fully clamped plate which was deformed by a crushing load applied by a rigid punch to the upper edge of the plate. This photograph is from full scale experiments conducted by S. Shimizu of Shimushu University in Japan.<sup>[10]</sup> Based on this photograph and other photographs of damage incurred by tankers during grounding accidents, the model for the local deformation mechanism shown in Figure 7 was developed.

The deformation of the web involves both bending and stretching. The bending of the web is caused by the formation of plastic hinge lines which are shown in Figure 7. The web deforms symmetrically about the point of application of the load. Six stationary plastic hinge lines form. Due to symmetry, only the three hinge lines on one side of the vertical plane of symmetry will be described. The first hinge line forms at the junction between the web and the upper flange. The second hinge line forms at an angle  $\alpha$  below the first hinge line. The third hinge line forms at an angle  $\beta$  below the second hinge line.

The photographs examined in developing this model showed the length of the deformed region in the longitudinal direction to be approximately twice the length in the vertical direction. This characteristic was included in the model by fixing the

angle between the upper edge of the undeformed web and the third hinge line at  $\pi/4$ . The vertical length of the deformed zone is taken as a parameter  $\zeta$ .

**3.2. DEFORMATION SEQUENCE:** Figure 8 depicts the geometry of the deformed web. The applied force  $P$ , causes the upper edge of the web to indent a distance  $\Delta$ . The angle of indentation is  $\theta_0$ . As  $\Delta$  increases the second hinge moves out of plane. The angle between the first and third hinges,  $\Phi$ , decreases. The angle between the vertical plane of symmetry and the third hinge line,  $\phi$ , remains constant at  $\pi/4$ .

The shaded area in Figure 8 illustrates the stretching in the deforming web. The attached flange deforms with the web as shown in Figure 9. Again, the shaded area illustrates the stretching in the deforming flange.

**3.3. LOAD-DEFLECTION RELATIONSHIP:** Following the Upper-Bound Theorem, the load deflection relationship is derived by equating the rate of external work performed in deforming the web girder to the rate of internal energy dissipation. In the following sections, this derivation is discussed. First the rate of internal energy dissipation is derived. Next, the rate of external work is formulated. Then, these two rates are equated to yield the load-deflection relationship.

3.3.1. RATE OF INTERNAL ENERGY DISSIPATION: The total rate of energy dissipation consists of two components-- that contributed from bending,  $\dot{E}_B$ , and that contributed from stretching,  $\dot{E}_M$ .

$$\dot{E}_{TOTAL} = \dot{E}_M + \dot{E}_B \quad (2)$$

3.3.1.1. BENDING ENERGY RATE: In general the bending energy rate term consists of energy dissipated by the continuous deformation field and energy dissipated by the discontinuous deformation field.

$$\dot{E}_B = \int_S M_o \dot{\kappa} dS + \sum_{i=1}^N M_o [\dot{\theta}_i] l_i \quad (3)$$

where S is the surface area of the deforming region;  $\dot{\kappa}$  is the rate of change of curvature;  $\dot{\theta}_i$  is the rate of rotation in the i'th hinge line; and  $l_i$  is the length of the i'th hinge line.

For the local denting model, however, the deformation is simplified by modelling all plastic hinges as stationary hinges. There is no continuous deformation field. The bending energy rate term simplifies to:

$$\dot{E}_B = 2 M_o \{ [\dot{\theta}_1] l_1 + [\dot{\theta}_2] l_2 + [\dot{\theta}_3] l_3 \} \quad (4)$$

where  $M_0$  is the fully plastic bending moment:

$$M_0 = \frac{\sigma_0 t_w^2}{4} \quad (5)$$

The assumption is made that all hinge lengths remain constant during the deformation process. The hinge lengths can be determined from the geometry of the model shown in Figure 6.

$$\begin{aligned} l_1 &= \zeta \\ l_2 &= \zeta / \cos(\alpha) \\ l_3 &= \sqrt{2} \zeta \end{aligned} \quad (6)$$

The rotation rates,  $\dot{\theta}_i$ , for each hinge line can be related to the angle  $\Phi$  between the first and third hinge lines. For each hinge line, a section normal to the hinge line is used to determine the rotation rate.

From the geometry of the model, the following can be determined:

$$\cos \theta_1 = \frac{\cos \beta - \cos \alpha \cos \Phi}{\sin \alpha \sin \Phi} \quad (7)$$

$$\cos \theta_2 = \frac{\cos \alpha - \cos \beta \cos \Phi}{\sin \beta \sin \Phi} \quad (8)$$

$$\cos \theta_3 = \frac{-\cos \alpha \cos \beta + \cos \Phi}{\sin \alpha \sin \beta} \quad (9)$$

Using the relationship that:

$$\frac{d}{dt} [\arccos(u)] = \frac{-\dot{u}}{\sqrt{(1-u^2)}} \quad (10)$$

with (7), (8), and (9), the rotation rates can be shown to be:

$$\dot{\theta}_1 = \frac{-\dot{\Phi} (\cos \alpha - \cos \beta \cos \Phi)}{\sin \Phi \sqrt{C_1 + C_2 \cos \Phi - \cos^2 \Phi}} \quad (11)$$

$$\dot{\theta}_2 = \frac{\dot{\Phi} \sin \Phi}{\sqrt{C_1 + C_2 \cos \Phi - \cos^2 \Phi}} \quad (12)$$

$$\dot{\theta}_3 = \frac{-\dot{\Phi} (\cos \beta - \cos \alpha \cos \Phi)}{\sin \Phi \sqrt{C_1 + C_2 \cos \Phi - \cos^2 \Phi}} \quad (13)$$

where:

$$\begin{aligned} C_1 &= (\sin^2 \alpha - \cos^2 \beta) \\ C_2 &= (2 \cos \alpha \cos \beta) \end{aligned} \quad (14)$$

By noting that the sum of the depression angle,  $\theta_3$ , and  $\Phi$  remains constant and equal to  $\pi/4$ ,  $\cos(\Phi)$ ,  $\sin(\Phi)$ , and  $\dot{\Phi}$  can be related to  $\Delta$  and  $\dot{\Delta}$ .

$$\cos\Phi = \frac{\sqrt{2}}{2} \frac{(\zeta + \Delta)}{\sqrt{\zeta^2 + \Delta^2}} \quad (15)$$

$$\sin\Phi = \frac{\sqrt{2}}{2} \frac{(\zeta - \Delta)}{\sqrt{\zeta^2 + \Delta^2}} \quad (16)$$

$$\dot{\Phi} = \frac{-\dot{\Delta} \zeta}{(\zeta^2 + \Delta^2)} \quad (17)$$

Substituting (11), (12), (13), and (6) into (4) yields:

$$\dot{E}_B = -2\zeta M_0 \dot{\Phi} \frac{(\cos^2\alpha - \cos\alpha\cos\beta\cos\Phi) + \sqrt{2}(\cos\alpha\cos\beta - \cos^2\alpha\cos\Phi) + 2\sin^2\Phi}{\cos\alpha \sin\Phi \sqrt{C_1 + C_2\cos\Phi - \cos^2\Phi}} \quad (18)$$

$$= -2 \zeta M_0 \dot{\Phi} \frac{(C_3 - C_4 \cos\Phi - \cos^2\Phi)}{\cos\alpha \sin\Phi \sqrt{C_1 + C_2 \cos\Phi - \cos^2\Phi}} \quad (19)$$

where

$$\begin{aligned} C_3 &= (\cos^2\alpha + \sqrt{2}\cos\alpha\cos\beta + 1) \\ C_4 &= (\sqrt{2}\cos^2\alpha + \cos\alpha\cos\beta) \end{aligned} \quad (20)$$

3.3.1.2. **MEMBRANE ENERGY RATE:** Now consider the membrane energy rate term of (2). Both the attached upper plating (or flange) and the web stretch while deforming.

Therefore:

$$\dot{E}_M \text{ total} = \dot{E}_M \text{ flange} + \dot{E}_M \text{ web} \quad (21)$$

The rate of membrane energy dissipation is defined as:

$$\dot{E}_M = \int_S N_o \dot{\epsilon} dS = \int_S N_o \dot{\epsilon} d\eta d\xi \quad (22)$$

where  $\dot{\epsilon}$  is the velocity strain in the deformed co-ordinates  $(\xi, \eta)$  and  $N_o$  is the fully plastic membrane force, defined below:

$$\dot{\epsilon} = \frac{d\dot{u}}{d\xi} \quad (23)$$

$$N_o = \sigma_o t \quad (24)$$

Integration of (22) yields:

$$\dot{E}_M = 2 N_o \int_0^{\eta_o} \dot{u} d\eta \quad (25)$$

where  $2\dot{u}$  is the velocity with which material points on either side of the centerline of the shaded regions shown in Figures 8 and 9 move apart relative to each other.

First, consider the stretching involved in deforming the flange. Figure 9 shows the trough shape of deformation that the flange assumes. Although the stretching of the flange occurs across the entire deformed region, the shaded area in Figure 9 is used to approximate the average strain involved. The amount of stretching is constant in the  $\xi$ -direction, normal to the longitudinal girder.

From the geometry of the model, it follows that:

$$u_f = \frac{\zeta}{\cos\theta_0} - \zeta = \frac{\sqrt{2}\zeta}{(\cos\Phi + \sin\Phi)} - \zeta \quad , \quad (26)$$

$$\dot{u}_f = \frac{-\sqrt{2}\dot{\Phi}\zeta(\cos\Phi - \sin\Phi)}{(1 + 2\cos\Phi\sin\Phi)} \quad . \quad (27)$$

Therefore,

$$\begin{aligned} \dot{E}_{M \text{ flange}} &= 2 \bar{N}_0 \int_0^B \dot{u} \, d\eta \\ &= -2\sqrt{2} \bar{N}_0 B \zeta \dot{\Phi} \frac{(\cos\Phi - \sin\Phi)}{(1 + 2\cos\Phi\sin\Phi)} \quad , \end{aligned} \quad (28)$$

where  $\bar{N}_o$  is the fully plastic membrane force for the flange:

$$\bar{N}_o = \sigma_o t_p \quad (29)$$

Now, consider the stretching involved in deforming the web. Again, the shaded region in Figure 8 can be used to approximate the average strain for the web. The amount of stretching varies along the depth of the web. The displacement  $u_f$  at the web flange connection and the maximum displacement  $u_x$  at the intersection of the second hinge lines are used to determine the average displacement as shown in Figure 10.

$$u_{web, avg} = \frac{1}{\zeta} \int_0^{\zeta \tan \alpha} \left[ u_f + \frac{(u_x - u_f) z}{\zeta \tan \alpha} \right] dz \quad (30)$$

$$+ \int_{\zeta \tan \alpha}^{\zeta} \left[ \frac{u_x (\zeta - z)}{\zeta (1 - \tan \alpha)} \right] dz$$

$$u_{web, avg} = \frac{1}{2} u_x + \frac{1}{2} \tan \alpha u_f \quad (31)$$

$$\dot{u}_{web, avg} = \frac{1}{2} \dot{u}_x + \frac{1}{2} \tan \alpha \dot{u}_f \quad (32)$$

From the geometry of the model, the following can be determined:

$$u_x = \zeta \frac{[(\sqrt{2} \cos\alpha - \cos\beta) \sin\Phi + \cos\beta \cos\Phi - \cos\alpha]}{[\cos\beta (\sin\Phi - \cos\Phi) + \cos\alpha]} \quad (33)$$

$$\dot{u}_x = -\sqrt{2} \dot{\Phi} \zeta \frac{(\cos\alpha \cos\beta - \cos^2\alpha \cos\Phi)}{[\cos\beta (\sin\Phi - \cos\Phi) + \cos\alpha]^2} \quad (34)$$

Substituting (27) and (33) into (31) and then substituting (31) into (25) yields:

$$\begin{aligned} \dot{E}_{M \text{ vab}} = -\sqrt{2} \dot{\Phi} \zeta^2 N_0 \left( \frac{(\cos\alpha \cos\beta - \cos^2\alpha \cos\Phi)}{[\cos\beta (\sin\Phi - \cos\Phi) + \cos\alpha]^2} \right. \\ \left. + \frac{\sin\alpha (\cos\Phi - \sin\Phi)}{\cos\alpha (1 + 2 \cos\Phi \sin\Phi)} \right) \quad (35) \end{aligned}$$

**3.3.2. RATE OF EXTERNAL WORK:** The rate of work done in deforming the structural unit is:

$$\dot{W}_{\text{ext}} = P_B \dot{\Delta} \quad (36)$$

Rearranging (17) and substituting this into (35) gives:

$$\dot{W}_{\text{ext}} = -P_B \dot{\Phi} \frac{(\zeta^2 + \Delta^2)}{\zeta} \quad (37)$$

3.3.3. **PHYSICAL LIMIT:** For the local denting mode,  $\alpha$  is modelled as a parameter. The choice of  $\alpha$  affects not only the magnitude of the crushing force for a specified crushing depth, but also the range of freedom for the model. The degree of freedom for the denting mode is exhausted when the upper flange makes contact with the "upper flap" of the web, the region between the first and second hinge lines. When this occurs,  $\theta_1 = \pi/2$  and :

$$\left(\frac{\Delta^*}{\zeta^*}\right)_{limit} = \frac{\cos^2\alpha + 2 \cos\beta \sqrt{\cos^2\alpha - \cos^2\beta}}{2 \cos^2\beta - \cos^2\alpha} \quad (38)$$

For approximately  $\alpha \leq \pi/12$ , the linear assumption discussed in Appendix A is valid. The load-deflection relationship in dimensionless terms is:

$$\begin{aligned} \frac{P_B}{M_0} &= \frac{2[(K_1 - K_2) - (K_2 + 2)\psi]}{\cos\alpha(1 - \psi) \sqrt{(K_3 - K_4) + (K_4 - 2)\psi}} \\ &+ \frac{2\sqrt{2} \zeta^* H^* [(K_5 - K_6) - K_6\psi]}{\cos^2\alpha - K_4\psi} \\ &+ \psi [4 \zeta^* H^* \tan\alpha + 8 B^* t^{*2}] \quad , \end{aligned} \quad (39)$$

where the dimensionless parameters are:

$$\begin{aligned} \Delta^* &= \frac{\Delta}{H} ; \quad \zeta^* = \frac{\zeta}{H} ; \quad H^* = \frac{H}{t_w} ; \\ B^* &= \frac{B}{t_p} ; \quad t^* = \frac{t_p}{t_w} \end{aligned} \quad (40)$$

and

$$\psi = \frac{\Delta^*}{\zeta^*} \quad (41)$$

The constants  $K_1$  through  $K_7$  are functions of  $\alpha$  and  $\beta$  which are listed in Appendix A (A6).

**3.3.4. INITIAL PHASE ENVELOPE:** For the local denting mode, it is postulated that the longitudinal and vertical extent of deformation,  $\zeta$ , is initially zero but spreads during the deformation process until the deformed region extends the depth of the web ( $\zeta = H$ ).

Figures 11 and 12 show the local denting solution for values of  $\zeta^*$  increasing from  $\zeta^* = 0.1$  to  $\zeta^* = 1.0$ . The parameters for the hull geometry ( $H^* = 100$ ;  $B^* = 75$ ;  $t^* = 1.0$ ) in both Figures 11 and 12 are approximate values for a 40,000 DWT USDH tanker. Figure 11 depicts the load-deflection curve for  $\alpha = \pi/12$ . The load-deflection curve for  $\alpha = \pi/8$  is shown in Figure 12.

Both Figures show envelopes for the initial phase of deformation. Due to the complexity of the load-deflection equation (39) it is difficult to analytically determine this envelope. The initial phase, however, may be described empirically by a function of the form:

$$\frac{P_B}{M_0} = C_0 (\Delta^*)^m \quad (42)$$

where the constant  $C_0$  and the exponent "m" depend on both the value of alpha and the geometric parameters describing the structure.

3.3.5. STRAIN AND STRAIN HARDENING: From the geometry of the model the strain averaged over the entire deforming area can be shown to be:

$$\epsilon_{avg} = \frac{1}{\left(B^*t^* + \frac{\zeta^*}{H^*}\right)} \left[ \left(B^*t^* + \frac{\zeta^*}{2h^*} \tan \alpha\right) \epsilon_f + \left(\frac{\zeta^*}{2h^*}\right) \epsilon_x \right] \quad (43)$$

where

$$\epsilon_f = \frac{\sqrt{2} - \cos \Phi - \sin \Phi}{(\cos \Phi + \sin \Phi)} \quad (44)$$

and

$$\epsilon_x = \frac{(\sqrt{2} \cos \alpha - \cos \beta) \sin \Phi + \cos \beta \cos \Phi - \cos \alpha}{[\cos \beta (\sin \Phi - \cos \Phi) + \cos \alpha]} \quad (45)$$

Strain hardening effects can be accounted for by adjusting the value of  $\sigma_0$  based on the average plastic strain. For example, if the stress-strain relationship for a given material

can be described by a power-law relationship similar to the Ramberg-Osgood formula <sup>(11)</sup>:

$$\sigma_o = \sigma_{ult} \left( \frac{\epsilon_{avg}}{\epsilon_{ult}} \right)^n \quad (46)$$

then, the following refinement of the denting model could be made:

$$\frac{P_B}{M_{ult}} = \left( \frac{\epsilon_{avg}}{\epsilon_{ult}} \right)^n \frac{P_B}{M_o} \quad (47)$$

where

$$M_U = \frac{\sigma_{ult} t_w^2}{4} \quad (48)$$

and  $P_B/M_o$  is defined by (39) or (A5).

## 4. GLOBAL BENDING MODE

4.1. **SIMPLIFIED MODEL:** This second mode of failure involves generation of a three hinge beam-bending mechanism, shown in Figure 13. For simplicity, the crushing load is applied at mid-span and the length between "hinge points" is equal. This mechanism could be adjusted to account for unequal lengths between hinge points.

The "hinge points" are modeled as shown in Figure 14. This model is similar to the local indentation model except there is no extension of the flange. The vertical extent of deformation,  $\zeta$ , extends the entire depth of the web; therefore,  $\zeta = H$ . Also, a fourth hinge line forms along the bottom flange at the centerline of the "hinge point" mechanism.

4.2. **DEFORMATION SEQUENCE:** Figures 13 & 14 show the web deforming in the global mode. The applied force  $P_c$  causes the legs of the three hinge mechanism to rotate an angle  $\gamma$ . This causes the angle  $\phi$  for each "hinge point" mechanism to decrease. The second hinge line moves out of plane and the angle between the first and third hinge lines,  $\Phi$ , decreases. This results in a local deflection,  $\delta$ , at the central "hinge point" mechanism. This local  $\delta$  is part of the total deflection  $\Delta$  as shown in Figure 13. The shaded area in Figure 15 illustrates the stretching of the web involved in deforming the "hinge point" mechanism.

The range of  $\Delta^*$  is limited to  $\Delta^* \leq 0.5$ . For a ship which may have a web girder depth on the order of 2 meters,  $\Delta^* = 0.5$  is a significant displacement of the hull. Because the range of  $\Delta^*$  is limited, the extension of the two "legs" of the global mechanism is neglected.

**4.3. LOAD-DEFLECTION RELATIONSHIP:** The application of  $P_1$  causes the three "hinge point" mechanisms to form. The "hinge point" mechanisms are separated by a distance  $(L/2 - H)$ . The central "hinge point" is designated the primary mechanism. The two outer "hinge points" are designated secondary mechanisms. The subscripts "p" and "s" are used to designate the primary and secondary mechanisms, respectively. As the central mechanism deflects, the two "legs" of the overall structure rotate an angle  $\gamma$ . From Figures 13 and 14, the angles  $\phi_p$  and  $\phi_s$  can be related to  $\gamma$ .

$$\phi_p = \frac{\pi}{4} - \gamma \quad (49)$$

and

$$\phi_s = \frac{\pi}{4} - \frac{\gamma}{2} \quad (50)$$

In the following sections, the internal rate of energy dissipation for the primary mechanism is formulated as a function of  $\gamma$  and  $\dot{\gamma}$ ,  $f_p(\gamma, \dot{\gamma})$ . In the global bending mode, energy is dissipated not only by the primary "hinge point" mechanism but also by the two secondary "hinge point" mechanisms. The total energy dissipated, therefore, is:

$$\dot{E}_{total} = f_p(\gamma, \dot{\gamma}) + 2f_s(\gamma, \dot{\gamma}) \quad , \quad (51)$$

where  $f_p$  and  $f_s$  are the functions formulated in the following sections for the total rate of internal energy dissipation for the primary and secondary "hinge point" mechanisms, respectively. The functions  $f_p$  and  $f_s$  are related by (49) and (50) so that:

$$f_s(\gamma, \dot{\gamma}) = f_p\left(\frac{\gamma}{2}, \frac{\dot{\gamma}}{2}\right) \quad . \quad (52)$$

**4.3.1. RATE OF INTERNAL ENERGY DISSIPATION:** The deformation of the web girder in the global bending mode, like that in the local denting mode, involves both bending and stretching. The expression for the internal rate of energy dissipation, therefore, is the same as stated by (2).

4.3.1.1. **BENDING ENERGY RATE:** Like the local denting model, the bending model consists of six stationary hinge lines in the web. In addition, one hinge line forms across the bottom flange as shown in Figure 13. There is no continuous deformation field. The bending energy rate term, therefore, is:

$$\dot{E}_{B_p} = 2M_O \{ l_1 [\dot{\theta}_{1p}] + l_2 [\dot{\theta}_{2p}] + l_3 [\dot{\theta}_{3p}] \} + \bar{M}_O l_4 [\dot{\theta}_{4p}] \quad (53)$$

where  $\bar{M}_O$  is the fully plastic bending moment for the flange:

$$\bar{M}_O = \frac{\sigma_o t_p^2}{4} \quad (54)$$

The assumption is made that the lengths of the hinge lines remain constant. From the geometry of the model, shown in Figure 14, the hinge line lengths can be determined:

$$\begin{aligned} l_1 &= H \\ l_2 &= H/\cos\alpha \\ l_3 &= \sqrt{2} H \\ l_4 &= H(1 - \tan\alpha) \\ l_5 &= B \end{aligned} \quad (55)$$

First, consider the fourth hinge line. The rotation rate of the fourth hinge line is simply:

$$\dot{\theta}_{4p} = 2 \dot{\gamma} \quad (56)$$

Now consider the other hinge lines. The rotation rates,  $[\dot{\theta}_i]$ , for the first, second and third hinge lines are related to the angle  $\Phi$  between the first and third hinge lines by the same relationships used for the local denting model--(11), (12) and (13). This is due to the similar geometry of the two models. The relationship of  $\Phi$  to  $\Delta$ , however, differs from that used for the local denting model.

To relate  $\Phi_p$  to  $\gamma$ , the following geometric relationships, which are evident from Figure 15, are used:

$$\Phi_p = \left( \frac{\pi}{2} - \phi_p \right) - \theta_o \quad (57)$$

$$\cos\theta_o = \sqrt{2} \sin\phi_p \quad (58)$$

$$\sin\theta_o = \sqrt{\cos^2\phi_p - \sin^2\phi_p} \quad (59)$$

$$\cos\Phi_p = \frac{\sqrt{2}}{2} \{ (1 - \sin 2\gamma) + (\cos\gamma + \sin\gamma) \sqrt{\sin 2\gamma} \} \quad (60)$$

$$\sin\Phi_p = \frac{\sqrt{2}}{2} \{ \cos 2\gamma - (\cos\gamma - \sin\gamma) \sqrt{\sin 2\gamma} \} \quad (61)$$

$$\dot{\Phi}_p = \frac{-2\dot{\gamma}(\sin 2\gamma \sqrt{\sin 2\gamma - \sin^2 2\gamma} + \cos 2\gamma (\frac{1}{2} - \sin 2\gamma))}{\sqrt{\sin 2\gamma - \sin^2 2\gamma} \sqrt{1 - \sin 2\gamma + 2\sin^2 2\gamma + 2\cos 2\gamma} \sqrt{\sin 2\gamma - \sin^2 2\gamma}} \quad (62)$$

In Appendix B, the  $\dot{E}_p$  term is presented as a function of  $\gamma$ .

**4.3.1.2. MEMBRANE ENERGY RATE:** The rate of membrane energy rate term is defined by (22) - (25). For the web, the maximum displacement,  $u_x$ , shown in Figure 15, is given by (32) with  $\zeta = H$ .

The average displacement,  $u_{web,avg}$  for the shaded region in Figure 15 is:

$$u_{web,avg} = \frac{1}{2} u_x \quad (63)$$

Differentiation of (63) and substitution of this into (25) yields:

$$\dot{E}_{M_p} = -\sqrt{2} \dot{\Phi}_p N_o H^2 \frac{\cos \alpha \cos \beta - \cos^2 \alpha \cos \Phi_p}{\{ \cos \beta (\sin \Phi_p - \cos \Phi_p) + \cos \alpha \}^2} \quad (64)$$

**4.3.1.3. SECONDARY MECHANISMS:** The internal rate of energy dissipation for the secondary mechanisms follows the same function as that for the primary mechanism evaluated at  $\gamma/2$ . Both the bending energy rate term and the membrane energy rate term for the secondary mechanisms are listed in Appendix B.

4.3.2. **RATE OF EXTERNAL WORK:** The rate of external work performed in deforming the web girder is:

$$\dot{W}_{ext} = P_B \dot{\Delta} \quad (65)$$

The local deflection,  $\delta$ , at the central mechanism can be described as a function of  $\gamma$  by considering the geometry of the model.

$$\delta = \sqrt{H^2 - 2H^2 \sin^2 \phi_p} = H \sqrt{\sin 2\gamma} \quad (66)$$

The total deflection,  $\Delta$ , is the sum of the local deflection and the deflection due to the rotation of the two legs of the entire mechanism.

$$\Delta = \delta + \left( \frac{L}{2} - H \right) \tan \gamma \quad (67)$$

Therefore

$$\dot{\Delta} = \dot{\delta} + \dot{\gamma} \left( \frac{L}{2} - H \right) \sec^2 \gamma \quad (68)$$

Differentiation of (66) and substitution of the result into (68) gives:

$$\dot{\Delta} = \frac{\dot{\gamma}}{2} \frac{ \{ H(\cos^2 \gamma - \sin^2 \gamma) \cos^2 \gamma + (L - 2H) \sqrt{\cos \gamma \sin \gamma} \} }{ \cos^2 \gamma \sqrt{\cos \gamma \sin \gamma} } \quad (69)$$

Substitution of this result into (65) gives:

$$\dot{W}_{ext} = (P_B H \dot{\gamma}) Z_T \quad , \quad (70)$$

where

$$\begin{aligned} Z_T &= \frac{\dot{\Delta}}{H \dot{\gamma}} \\ &= \frac{1}{2} \frac{(\cos^2\gamma - \sin^2\gamma) \cos^2\gamma + \left(\frac{L}{H} - 2\right) \sqrt{\cos\gamma \sin\gamma}}{\cos^2\gamma \sqrt{\cos\gamma \sin\gamma}} \end{aligned} \quad (71)$$

4.3.3. **PHYSICAL LIMIT:** As in the local denting mode,  $\alpha$  is modelled as a parameter for the global bending mode also. The choice of  $\alpha$  affects not only the magnitude of the crushing force for a specified crushing depth, but also the range of freedom for the model. The degree of freedom for the bending mode is exhausted when the connection of the web to the flange moves out of the Z-Y plane. This occurs when:

$$\gamma_{limit} = \frac{\pi}{4} - \arctan \left( 1 - \frac{\sin^2\alpha}{\sin^2\beta} \right)^{\frac{1}{2}} \quad . \quad (72)$$

4.3.4. GLOBAL LOAD-DEFLECTION RELATIONSHIP: In Appendix B, the external rate of work is equated to the total rate of internal energy dissipation for both the primary mechanism and the two secondary mechanisms. The dimensionless equation for  $P_B/M_0$  is:

$$\begin{aligned} \frac{P_B}{M_0} = & \frac{4Z_p}{Z_T} \left( \frac{C_3 - C_4 \cos \Phi_p - \cos^2 \Phi_p}{\cos \alpha \sin \Phi_p \sqrt{C_1 + C_2 \cos \Phi_p - \cos^2 \Phi_p}} + \frac{2\sqrt{2}H^* (\cos \alpha \cos \beta - \cos^2 \alpha \cos \Phi_s)}{(\cos \beta (\sin \Phi_p - \cos \Phi_p) + \cos \alpha)^2} \right) \\ & + \\ & \frac{8Z_s}{Z_T} \left( \frac{C_3 - C_4 \cos \Phi_s - \cos^2 \Phi_s}{\cos \alpha \sin \Phi_s \sqrt{C_1 + C_2 \cos \Phi_s - \cos^2 \Phi_s}} + \frac{2\sqrt{2}H^* (\cos \alpha \cos \beta - \cos^2 \alpha \cos \Phi_s)}{(\cos \beta (\sin \Phi_s - \cos \Phi_s) + \cos \alpha)^2} \right) \\ & + \frac{4B^* t^3}{Z_T H^*} \end{aligned} \quad (73)$$

where

$$\Delta^* = \sqrt{2} (\gamma)^{\frac{1}{2}} + \left( \frac{L^*}{2} - 1 \right) \gamma \quad (74)$$

and the a new dimensionless parameter is introduced:

$$L^* = \frac{L}{H} \quad (75)$$

The expression for  $Z_r$  is given in (71). The expressions for  $Z_p$ ,  $\text{COS } \Phi_p$ , and  $\text{SIN } \Phi_p$  are given by (B2), (B3) and (B4) respectively. The expressions for  $Z_s$ ,  $\text{COS } \Phi_s$ , and  $\text{SIN } \Phi_s$  are given by (B6), (B7), and (B8), respectively. The dimensionless parameters are listed in (39) and a new dimensionless parameter is introduced:

For small values of  $\gamma$ , small angle approximations can be employed and higher order terms can be neglected. Because the extension of the two "legs" of the global bending mechanism is neglected,  $\Delta^*$  is limited to  $\Delta^* \leq 0.5$ . Over this range of  $\Delta^*$ ,  $\gamma \leq 5$  degrees for values of  $H^*$  and  $L^*$  which are reasonable for ship scantlings. Applying small angle approximations and neglecting higher order simplifies the following:

$$\begin{aligned}
 \text{COS } \Phi_p &= \frac{\sqrt{2}}{2} + (\gamma)^{\frac{1}{2}} - \sqrt{2}(\gamma) + (\gamma)^{\frac{3}{2}} \\
 \text{SIN } \Phi_p &= \frac{\sqrt{2}}{2} - (\gamma)^{\frac{1}{2}} + (\gamma)^{\frac{3}{2}} \\
 Z_p &= \frac{\sqrt{2} \left\{ \frac{1}{2} - 2\gamma + 2\sqrt{2}\gamma^{\frac{3}{2}} \right\}}{\left\{ \gamma + 2\gamma^{\frac{3}{2}} \right\}^{\frac{1}{2}}}
 \end{aligned}
 \tag{76}$$

$$\begin{aligned}\cos\Phi_s &= \frac{\sqrt{2}}{2} \left( 1 - (\gamma) + (\gamma)^{\frac{1}{2}} + \frac{1}{2} (\gamma)^{\frac{3}{2}} \right) \\ \sin\Phi_s &= \frac{\sqrt{2}}{2} \left( 1 - (\gamma)^{\frac{1}{2}} + \frac{1}{2} (\gamma)^{\frac{3}{2}} \right) \\ Z_s &= \frac{2 \left\{ \frac{1}{2} - \gamma + \gamma^2 \right\}}{\left( \gamma + 2\gamma^{\frac{3}{2}} - 2\gamma^2 \right)^{\frac{1}{2}}}\end{aligned}\tag{77}$$

$$\begin{aligned}Z_T &= \frac{\sqrt{2} + (L^* - 2) (\gamma)^{\frac{1}{2}}}{2 (\gamma)^{\frac{1}{2}}} \\ \Delta^* &= \sqrt{2} (\gamma)^{\frac{1}{2}} + \left( \frac{L^*}{2} - 1 \right) (\gamma)\end{aligned}\tag{78}$$

**4.3.5. STRAIN HARDENING:** Strain hardening effects may be included in the global bending model in the same manner in which they were included for the local denting model in section 3.3.5. For the global bending model,  $P_s/M_o$  in equation (47) is represented by (73).

**4.4. COMBINED BENDING-DENTING MODEL:** Figures 16 and 17 show the combined local denting and global bending load-deflection curves for typical parameters for a 40,000 DWT USDH tanker. Figure 16 is the load-deflection curve for  $\alpha = \pi/12$ . The curve for  $\alpha = \pi/8$  is shown in Figure 17. Both Figure indicate transitions from the local denting mode to the global bending mode where the two solutions cross.

## 5. CRUSHING EXPERIMENTS

5.1. BACKGROUND: Four extruded aluminium double hollow sections were crushed for this study. Two experiments were set-up to initiate the local denting mode. The other two experiments were designed to simulate the global bending mode. Appendix C contains descriptions of the experiments.

The depth-to-thickness ratio for these specimens was  $H/t_w = 20.3$ , which is at the lower end of the thin-wall member spectrum. Also, the material exhibited significant strain-hardening properties. Appendix D contains the specification of the aluminium specimens that were crushed.

The extruded aluminium specimens were provided by Reynolds Aluminium, Holland B.V. This size of extruded shape was used in order to maintain a small scale which could easily be handled with standard laboratory machines. The specimens were 300 mm long, 127 mm wide, and 50.8 mm deep. The issue of structural discontinuity and inhomogeneity due to welds was avoided by using extruded forms.

The double hollow profile was chosen in order to provide some restraint against in-plane motion in the transverse direction. A multiple cell section such as that shown in Figure 5 would have been an ideal choice. The double hollow form, however, was selected due to availability.

5.2. LOCAL DENTING: Figures 18 and 19 show the load-deflection curves for the two denting experiments. A photograph of the deformed specimen from the first denting experiment is shown in Figure 20.

5.2.1. DESCRIPTION OF DEFORMATION: Due to the significant strain hardening effects, it was difficult to see the propagation of the deformation during the crushing process. The photograph in Figure 20 shows the permanent deformation of the first dented specimen with one of the outer webs cut away to expose the interior web. The pattern of deformation is very similar to that postulated for the simplified model. The angle  $\alpha$  between the flange-web connection and the first hinge line is approximately 15 degrees. The shape of the lower hinge line is parabolic rather than straight. The longitudinal length of the deformed region, however, is approximately twice the depth of the web.

In both denting experiments, fracture occurred at the juncture of the outer two webs and the upper flange. During the crushing process, the location of fracture was obscured by the rigid punch. Therefore, the crushing depth ( $\Delta^*$ ) at which fracture began was not recorded.

Both denting specimens showed initial signs of fracture along the second hinge line. This appears to be a result of the fact that a structure cannot assume infinitely small radii of curvature. Because the local denting model employs stationary

hinges and is formulated for only a discontinuous deformation field, this feature is not included in the model.

The ends of the specimens for both denting experiments were clamped to the work surface only at the lower flange. A fully clamped condition was not achieved. A small degree of "pull-in" in the longitudinal direction was observed during the crushing process. The local denting model solution was developed with the assumption of fully clamped ends. The amount of energy dissipated by stretching in the experiments was probably less than that predicted by the simplified model.

**5.2.2. LOAD-DEFLECTION CURVES:** The load-deflection curves labeled "MODEL" in Figures 18 and 19 were developed from Equation (A5) with the parameters listed below. The curves shown are the envelopes of the curves produced by (A5). Each specimen was modelled as three structural units with the following geometric parameters:

$$\begin{array}{ll} \alpha = \pi/12 & H^* = 20.3 \\ B^* = 16.9 & t^* = 1.0 \end{array}$$

Although the two outer structural units are channel type sections rather than I-beam type sections, it is assumed that the two outer webs deform in the same manner as the inner web during the crushing process.

Strain hardening effects were included as discussed in section (3.3.3). The stress-strain curve for the specimens which was provided by the manufacturer is included in Appendix D.

As shown in Figures 18 and 19, the local denting model over-predicts the energy absorbed in the crushing process. It also does not capture the load reduction which occurs at approximately  $\Delta^* = 0.10$ . The model shows an almost linear increase in load after the initial phase. Some of the load reduction may be due to the lack of fully clamped end conditions.

From the derivations in Appendix A, it can be shown that the membrane energy involved in stretching the flange is the most significant factor in this region of the load-deflection curve. The relative magnitude of the crushing load for the model and the general character of the curves, however, show good agreement with the experimental results.

**5.3. GLOBAL BENDING MODE:** Figures 21 and 22 show the load-deflection curves for the two bending experiments. Figure 23 is a photograph of the deformed specimen from the first bending experiment.

5.3.1. DESCRIPTION OF DEFORMATION: Again, the photograph in Figure 23 shows the permanent deformation viewed after experiments were completed. The deformation is similar to that postulated for the bending model. The angle  $\alpha$  is approximately 22 degrees. The parabolic shapes of the hinge lines are more pronounced in these specimens than in those of the denting experiments.

In the first bending experiment, fracture occurred at the juncture of the two outer webs with the upper flange. The second bending experiment was halted at a smaller value of  $\Delta^*$ . The initiation of fracture is evident at the same locations for this specimen.

5.3.2. LOAD-DEFLECTION CURVES: Figures 21 and 22 show the load-deflection curves for the bending experiments. The curves labeled "BENDING MODEL" and "DENTING MODEL" were developed from the models discussed in sections 3 and 4 with strain hardening effects included as discussed in sections 3.3.5 and 4.3.5.

The specimens were modelled as three structural units with the following geometric parameters:

$$\begin{aligned} \alpha &= \pi / 8 & H^* &= 20.3 \\ B^* &= 16.9 & t^* &= 1.0 \\ L^* &= 4.4 \end{aligned}$$

The global bending mode was treated as bending of a free beam. The contributions from the secondary hinge mechanisms were neglected.

The theoretical model for the bending mode shows very close agreement with the experimental results both in the shape and the magnitude of the load-deflection curves. The theoretical denting model, however, over-predicts the required force during the initial phase prior to transition to overall bending.

## 6. CONCLUSIONS & RECOMMENDATIONS

The objective of this study was to investigate the crushing characteristics of web girders for a USDH structure. The crushing experiments that were conducted provide more insight into the shape of the deformation that a web girder undergoes when subjected to a concentrated lateral collapse load. The shapes of the deformed specimens shown in Figures 20 and 23 are very similar to the photograph in Figure 6 which shows damage to a fully clamped plate subjected to a crushing load.

The local denting model over-predicted the amount of energy absorbed for the denting experiments. A model with a continuous deformation field may better predict the initial phase for the denting solution.

From the derivations of the load-deflection for the denting model, it can be seen that the energy involved in stretching the flange is the most significant term contributing to the total rate of internal energy dissipation. The bending energy and the energy involved in stretching the web are negligible in comparison. Denting experiments with fully clamped end conditions would provide better insight into the stretching involved in deforming the flange plating. Also, experiments using thinner specimens (greater depth-to-thickness ratios) with less significant strain hardening characteristics would provide more insight into the initial mode of deformation and any transition to different modes of deformation.

The theoretical load-deflection curve for the global bending model closely followed the experimental results for a structural unit with free-free end conditions. The shape of the load-deflection curve for the global bending model is very similar to the shape of experimental results presented by de Oliveira <sup>[12]</sup> for a horizontally free circular tube subjected to a concentrated lateral crushing load.

The membrane energy involved in the extension of the two "legs" of the bending mechanism was neglected for the theoretical model. This may be a significant factor for a fully clamped structural unit. Crushing experiments for fully clamped conditions would be worthwhile.

The models presented in this paper were based on stationary straight hinge lines. Although the actual hinge lines are parabolic curves, the models provide reasonable estimates of the energy absorbed during the crushing process. For a given set of geometric parameters ( $H^*$ ,  $B^*$ ,  $T^*$ , and  $L^*$ ), the formulas developed for these models could be approximated by simple functions and then incorporated in damage prediction models. For example, a linearly increasing function could be used to approximate the local crushing solution. For the combined denting-bending mode, a mean crushing force could be employed. These simple functions could be used to describe the springs of the USDH model shown in Figure 3. The denting model could be used to describe the vertical springs. The global bending model could be used to describe the diagonal springs.

For this study, several assumptions were made in order to keep the analysis of the crushing characteristics relatively simple and mathematically tractable. These assumptions may require further investigation.

In particular, the assumption that there is no load-interaction between bending moments and membrane forces was made to uncouple the energy dissipation terms. The inclusion of the interaction surface for the different forces would make the problem significantly more difficult, as pointed out by de Oliveira <sup>[13]</sup>.

A further refinement of the models presented in this paper could be made for the method of including strain hardening effects. Strain hardening was accounted for by a relatively crude manner which utilized the average strain over the entire structure. The strain for each deforming region could be used to adjust the flow stress for each region.

Another factor which requires further investigation is fracture. Not only may fracture affect the deformation mode and the load carrying capacity of a web girder unit, it may also initiate flooding in a ship's double hull. For the models, an estimate of initial fracture could be made based using a critical strain to rupture criteria for the regions of maximum strain.

For the crushing experiments, fracture first occurred at the upper web flange connections for the outer flanges. The ultimate strain for the experimental specimens was on the order

of 20%. Strain in this connection region should be investigated. The extruded shapes had stress concentrations in this region due to the geometry shown in Figure 26. A USDH ship structure, also, will have stress concentrations due to welded joints.

## REFERENCES

- <sup>1</sup> Tomiyasu Okamoto et al., "Strength Evaluation of Novel Unidirectional Girder System Product Oil Carrier by Reliability Analysis," SNAME Transactions, 93 (1985), pp. 55-77.
- <sup>2</sup> Jeffery E. Beach, "Advanced Surface Ship Hull Technology-- Cluster B," Naval Engineer's Journal, Vol. 103 No. 6 (Nov 91), pp 28-31.
- <sup>3</sup> John F. McDermott et al., "Tanker Structural Analysis for Minor Collisions," SNAME Transactions, 89 (1974), pp. 382-407.
- <sup>4</sup> Pin Yu Chang, review of "Tanker Structural Analysis for Minor Collisions," by McDermott et al., SNAME Transactions, 89 (1974) p. 408.
- <sup>5</sup> Tomasz Wierzbicki et al., "Damage Estimates in High Energy Groundings," Report No. 1: Joint M.I.T.-Industry Program on Safe Tankers, pp. 51-56.
- <sup>6</sup> Tomasz Wierzbicki, "Progressive Damage and Rupture of Unidirectionally Stiffened Double Hulls Resulting from Underwater Explosions," Research proposal submitted to David Taylor Research Center, December 91, p. 10.
- <sup>7</sup> W. Johnson and S. R. Reid, "Metallic Energy Dissipating Systems," Applied Mechanics Review, Vol. 31, No. 3 (1978), pp. 277-288.
- <sup>8</sup> De Oliviera, T. Wierzbicki, and W. Abramowicz, "Plastic Behavior of Tubular Members under Lateral Concentrated Loading," Det Norske Veritas Technical Report No. 82-0708 (Progress Report July 30, 1982) pp. 1-4.
- <sup>9</sup> C. R. Calladine, Plasticity for Engineers (Chichester, England: Ellis Horwood Ltd., 1985) p. 104.
- <sup>10</sup> Private communications between T. Wierzbicki and S. Shimizu of Shimushu University.
- <sup>11</sup> Jacob Lubliner, Plasticity Theory (New York: MacMillian Publishing Co., 1990) pp. 74-75.
- <sup>12</sup> De Oliviera, T. Wierzbicki, and W. Abramowicz, "Plastic Behavior of Tubular Members under Lateral Concentrated Loading," Det Norske Veritas Technical Report No. 82-0708 (Progress Report July 30, 1982) pp. 38-39.

REFERENCES, CONT'D

<sup>13</sup> De Oliviera, T. Wierzbicki, and W. Abramowicz, "Plastic Behavior of Tubular Members under Lateral Concentrated Loading," Det Norske Veritas Technical Report No. 82-0708 (Progress Report July 30, 1982) p. 39.

## BIBLIOGRAPHY

Beach, Jeffery E. "Advanced Surface Ship Hull Technology-- Cluster B." Naval Engineer's Journal, Vol. 103 No. 6 (Nov 91).

Calladine, C.R. Plasticity for Engineers. Chichester, England: Ellis Horwood Ltd., 1985.

Chang, Pin Yu. review of "Tanker Structural Analysis for Minor Collisions." by McDermott et al. SNAME Transactions, 89 (1974).

De Oliviera, T. Wierzbicki, and W. Abramowicz. "Plastic Behavior of Tubular Members under Lateral Concentrated Loading," Det Norske Veritas Technical Report No. 82-0708 (Progress Report July 30, 1982).

Johnson, W. and S. R. Reid. "Metallic Energy Dissipating Systems." Applied Mechanics Review, Vol. 31, No. 3 (1978).

Lubliner, Jacob. Plasticity Theory. New York: MacMillian Publishing Co., 1990.

McDermott, John F. et al. "Tanker Structural Analysis for Minor Collisions." SNAME Transactions, 89 (1974).

Okamoto, Tomiyasu et al. "Strength Evaluation of Novel Unidirectional Girder System Product Oil Carrier by Reliability Analysis." SNAME Transactions, 93 (1985).

Wierzbicki, Tomasz. "Progressive Damage and Rupture of Unidirectionally Stiffened Double Hulls Resulting from Underwater Explosions." Research proposal submitted to David Taylor Research Center, December 91.

Wierzbicki, Tomasz et al. "Damage Estimates in High Energy Groundings." Report No. 1: Joint M.I.T.-Industry Program on Safe Tankers.

## APPENDIX A: LOCAL DENTING MODE

In this section the development and the normalization of the load-deflection relationship for the local denting mode is detailed.

**A.1. LOAD-DEFLECTION RELATIONSHIP:** Equating the external rate of work to the internal rate of energy dissipation gives:

$$\dot{W}_{ext} = \dot{E}_{total} = \dot{E}_B + \dot{E}_{M flange} + \dot{E}_{M web} \quad (A1)$$

Substituting (37), (19), (28), and (35) into (A1) and making dimensionless yields:

$$\begin{aligned} \frac{P_B}{M_0} = \frac{\zeta^{*2}}{(\zeta^{*2} + \Delta^{*2})} & \left( \frac{2 (C_3 - C_4 \cos \Phi - \cos^2 \Phi)}{\cos \alpha \sin \Phi \sqrt{C_1 + C_2 \cos \Phi - \cos^2 \Phi}} \right. \\ & + 4\sqrt{2} \zeta^* H^* \left[ \frac{(\cos \alpha \cos \beta - \cos^2 \alpha \cos \Phi)}{(\cos \beta (\sin \Phi - \cos \Phi) + \cos \alpha)^2} \right. \\ & \quad \left. \left. \frac{\sin \alpha (\cos \Phi - \sin \Phi)}{\cos \alpha (1 + 2 \cos \Phi \sin \Phi)} \right] \right) \\ & + 8\sqrt{2} B^* t^{*2} \frac{(\cos \Phi - \sin \Phi)}{(1 + 2 \cos \Phi \sin \Phi)} \quad (A2) \end{aligned}$$

where

$$\begin{aligned}\cos\Phi &= \frac{\sqrt{2}}{2} \frac{(\zeta^* + \Delta^*)}{\sqrt{\zeta^{*2} + \Delta^{*2}}} \\ \sin\Phi &= \frac{\sqrt{2}}{2} \frac{(\zeta^* - \Delta^*)}{\sqrt{\zeta^{*2} + \Delta^{*2}}}\end{aligned}\tag{A3}$$

The dimensionless parameters variables are:

$$\begin{aligned}\Delta^* &= \frac{\Delta}{H} ; \quad \zeta^* = \frac{\zeta}{H} ; \quad H^* = \frac{H}{t_v} ; \\ B^* &= \frac{B}{t_p} ; \quad t^* = \frac{t_p}{t_v}\end{aligned}\tag{A4}$$

Substituting (A3) into (A2) yields:

$$\begin{aligned}\frac{P_B}{M_0} &= \frac{1}{1 + \psi^2} \left( \frac{2[K_1(1+\psi^2) - 2\psi - K_2(1+\psi)(1+\psi^2)^{1/2}]}{\cos\alpha(1-\psi)\sqrt{K_3(1+\psi^2) - 2\psi + K_4(1+\psi)(1+\psi^2)^{1/2}}} \right) \\ &+ \frac{2\sqrt{2}\zeta^*H^*}{1 + \psi^2} \left( \frac{[K_5(1+\psi^2) - K_6(1+\psi)(1+\psi^2)^{1/2}]}{[K_7\psi^2 - K_4\psi(1+\psi^2)^{1/2} + \cos\alpha]} \right) \\ &+ \left( \frac{(4\zeta^*H^*t^*\tan\alpha + 8B^*t^{*2})}{1 + \psi^2} \right) \psi(1 + \psi^2)^{1/2}\end{aligned}\tag{A5}$$

$$\begin{aligned}K_1 &= 2\cos^2\alpha + 2\sqrt{2}\cos\alpha\cos\beta + 1 \\ K_2 &= 2\cos^2\alpha + \sqrt{2}\cos\alpha\cos\beta \\ K_3 &= 1 - 2(\cos^2\alpha - \cos^2\beta) \\ K_4 &= 2\sqrt{2}\cos\alpha\cos\beta \\ K_5 &= 2\cos\alpha\cos\beta \\ K_6 &= \sqrt{2}\cos\alpha \\ K_7 &= 2\cos^2\beta + \cos^2\alpha\end{aligned}\tag{A6}$$

$$\psi = \frac{\Delta^*}{\zeta^*} \quad (\text{A7})$$

If  $\psi < 1$ , then  $\psi^2 \ll 1$ . If this case holds, then Equation (A5) can be linearized by neglecting  $\psi^2$ . Equation (A5) becomes:

$$\begin{aligned} \frac{P_B}{M_0} = & \left( \frac{2 [ (K_1 - K_2) - (K_2 + 2)\psi ]}{\cos\alpha (1 - \psi) \sqrt{(K_3 - K_4) + (K_4 - 2)\psi}} \right) \\ & + \left( \frac{2\sqrt{2} \zeta^* H^* [ (K_5 - K_6) - K_6 \psi ]}{\cos^2\alpha - K_4 \psi} \right) \\ & + ( \psi [ 4 \zeta^* H^* \tan\alpha + 8 B^* t^{*2} ] ) \end{aligned} \quad (\text{A8})$$

## APPENDIX B: GLOBAL BENDING MODE

**B.1. BENDING ENERGY RATE:** Substitution of (60), (61), and (62) into (11), (12), and (13) gives expressions for  $[\theta_1]$ ,  $[\theta_2]$ , and  $[\theta_3]$  in terms of  $\gamma$ . Substitution of these expressions and (55), and (56) into (53) yields:

$$\dot{E}_{B_p} = 2 \dot{\gamma} M_0 H Z_p \left( \frac{C_3 - C_4 \cos \Phi_p - \cos^2 \Phi_p}{\cos \alpha \sin \Phi_p \sqrt{C_1 + C_2 \cos \Phi_p - \cos^2 \Phi_p}} \right) + 2 B \bar{M}_0 \dot{\gamma} \quad (\text{B1})$$

where  $C_1$ , and  $C_2$  are given by (14);  $C_3$ , and  $C_4$  are given by (20); and:

$$Z_p = \frac{-\frac{\dot{\Phi}_p}{\dot{\gamma}}}{\frac{2 (\sin 2\gamma \sqrt{\sin 2\gamma - \sin^2 2\gamma} + \cos 2\gamma (\frac{1}{2} - \sin 2\gamma))}{(\sin 2\gamma - \sin^2 2\gamma)^{\frac{1}{2}} (1 - \sin 2\gamma + 2 \sin^2 2\gamma + 2 \cos 2\gamma \sqrt{\sin 2\gamma - \sin^2 2\gamma})^{\frac{1}{2}}}} \quad (\text{B2})$$

$$\cos \Phi_p = \frac{\sqrt{2}}{2} \{ (1 - \sin 2\gamma) + (\cos \gamma + \sin \gamma) \sqrt{\sin 2\gamma} \} \quad (\text{B3})$$

$$\sin \Phi_p = \frac{\sqrt{2}}{2} \{ \cos 2\gamma - (\cos \gamma - \sin \gamma) \sqrt{\sin 2\gamma} \} \quad (\text{B4})$$

**B.2. SECONDARY HINGE MECHANISMS:** The bending energy rate terms and the membrane energy rate terms for the secondary mechanisms are equal to those for the primary mechanism evaluated at  $\gamma/2$  rather than  $\gamma$ . The bending energy rate term is:

$$\dot{E}_B = 2 \dot{\gamma} M_0 H Z_s \left( \frac{C_3 - C_4 \cos \Phi_s - \cos^2 \Phi_s}{\cos \alpha \sin \Phi_s \sqrt{C_1 + C_2 \cos \Phi_s - \cos^2 \Phi_s}} \right) + B \overline{M_0} \dot{\gamma} \quad (\text{B5})$$

where

$$Z_s = \frac{\dot{\Phi}_s}{-\dot{\gamma}} = \frac{2 \{ \sin \gamma \sqrt{\sin \gamma - \sin^2 \gamma} + \cos \gamma \left( \frac{1}{2} - \sin \gamma \right) \}}{\{ \sin \gamma - \sin^2 \gamma \}^{\frac{1}{2}} \{ 1 - \sin \gamma + 2 \sin^2 \gamma + 2 \cos \gamma \sqrt{\sin \gamma - \sin^2 \gamma} \}^{\frac{1}{2}}} \quad (\text{B6})$$

$$\cos \Phi_s = \frac{\sqrt{2}}{2} \{ (1 - \sin \gamma) + (\sin \gamma + \sin^2 \gamma)^{\frac{1}{2}} \} \quad (\text{B7})$$

$$\sin \Phi_s = \frac{\sqrt{2}}{2} \{ \cos \gamma - (\sin \gamma - \sin^2 \gamma)^{\frac{1}{2}} \} \quad (\text{B8})$$

The membrane energy rate term for the secondary mechanisms is:

$$\dot{E}_{M_s} = -\sqrt{2} \dot{\Phi}_s N_0 H^2 \frac{\cos\alpha\cos\beta - \cos^2\alpha\cos\Phi_s}{(\cos\beta(\sin\Phi_s - \cos\Phi_s) + \cos\alpha)^2} \quad (B9)$$

**B.3. LOAD—DEFLECTION RELATIONSHIP:** The total internal rate of energy dissipation consists of the energy rate terms for the one primary mechanism and the energy rate terms for the two secondary mechanisms. Combining these terms, equating the sum to the external rate of work, and making dimensionless yields:

$$\begin{aligned} \frac{P_B}{M_0} = & \frac{4Z_p}{Z_T} \left( \frac{C_3 - C_4 \cos\Phi_p - \cos^2\Phi_p}{\cos\alpha \sin\Phi_p \sqrt{C_1 + C_2 \cos\Phi_p - \cos^2\Phi_p}} + \frac{2\sqrt{2}H^* (\cos\alpha\cos\beta - \cos^2\alpha\cos\Phi_s)}{(\cos\beta(\sin\Phi_p - \cos\Phi_p) + \cos\alpha)^2} \right) \\ & + \\ & \frac{8Z_s}{Z_T} \left( \frac{C_3 - C_4 \cos\Phi_s - \cos^2\Phi_s}{\cos\alpha \sin\Phi_s \sqrt{C_1 + C_2 \cos\Phi_s - \cos^2\Phi_s}} + \frac{2\sqrt{2}H^* (\cos\alpha\cos\beta - \cos^2\alpha\cos\Phi_s)}{(\cos\beta(\sin\Phi_s - \cos\Phi_s) + \cos\alpha)^2} \right) \\ & + \frac{4B^* t^{*3}}{Z_T H^*} \end{aligned} \quad (B10)$$

where

$$\Delta^* = \sqrt{2} (\gamma)^{\frac{1}{2}} + \left( \frac{L^*}{2} - 1 \right) \gamma \quad (\text{B11})$$

The dimensionless parameters are listed in (39) and a new dimensionless parameter is introduced:

$$L^* = \frac{L}{H} \quad (\text{B12})$$

## APPENDIX C: EXPERIMENT SET-UP

**C.1. DENTING EXPERIMENTS:** Figure 24 shows a side-view and an end-view of the set-up for the denting experiments. The specimens were clamped to the work surface only along the lower flange. The work surface (the platen) was raised in a displacement control mode and the reaction force  $P_r$  was measured as a function of displacement. A solid steel cylinder 25 mm diameter was used as the rigid punch. The solid cylinder was used rather than a knife-edge indenter to delay initiation of fracture.

**C.2. BENDING EXPERIMENTS:** Figure 25 shows a side-view and an end-view of the set-up for the bending experiments. A three-point bending set-up was used. The specimens were not clamped. Instead, bending of a free beam was modelled. The specimens were placed on two steel rods of 25 mm diameter that were spaced 225 mm apart. A third steel rod was connected to the load-cell above the specimens. The base was raised in a displacement control mode and the reaction force  $P_r$  was measured as a function of displacement.

## APPENDIX D: EXPERIMENT SPECIMEN SPECIFICATIONS

D.1. DIMENSIONS: Figure 26 shows a cross-section and the dimensions of the prismatic specimens used for the crushing experiments.

D.2. MATERIAL PROPERTIES: The specimens used for the crushing experiments were extruded 6061 aluminium which were supplied by Reynolds Aluminium Holland, B.V. The material properties for the specimens are listed in Table D-1, below.

TABLE D-1: MATERIAL PROPERTIES

YOUNG'S MODULUS	69 GPa
YIELD STRESS	114 MPa
ULTIMATE STRESS	220 MPa
ULTIMATE STRAIN	0.206
BRINELL HARDNESS	69

The material has significant strain hardening properties. In order to incorporate this characteristic in the theoretical models, the stress-strain curve was modelled as:

$$\sigma = \sigma_{ult} \left( \frac{\epsilon}{\epsilon_{ult}} \right)^n \quad (D1)$$

with  $n = 0.165$ ;  $\sigma_0 = 220$  MPa; and  $\epsilon_{ult} = 0.206$ .

The points plotted in Figure 27 were obtained from the tensile stress-strain curve provided by the supplier. The curve shown in Figure 27 is the power-law model which was used for the theoretical model solutions.

FIGURES

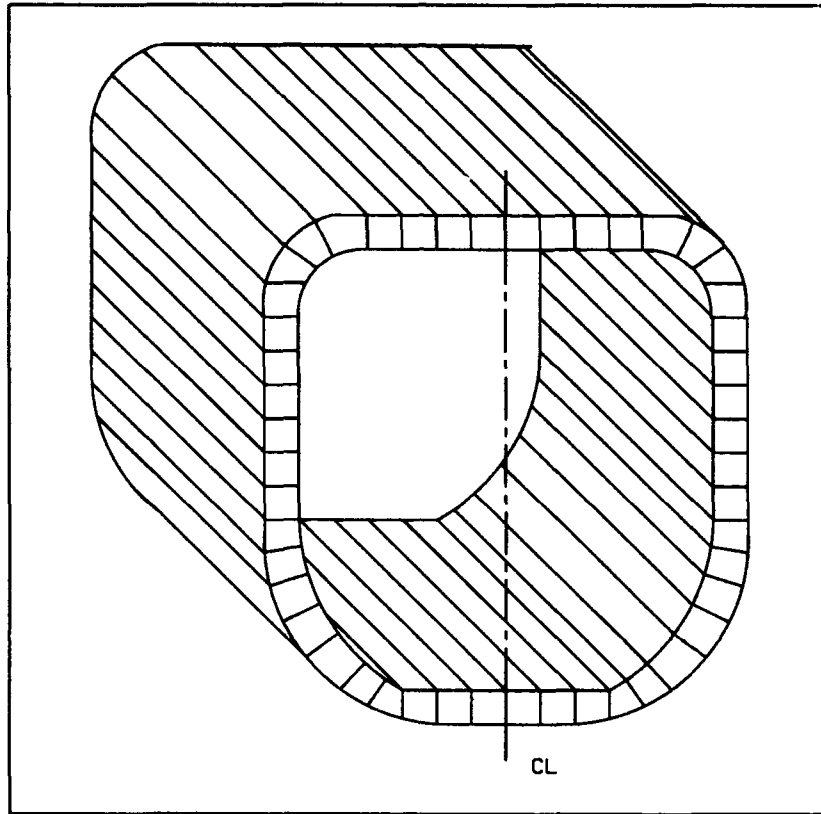


Figure 1: The USDH Hull Form

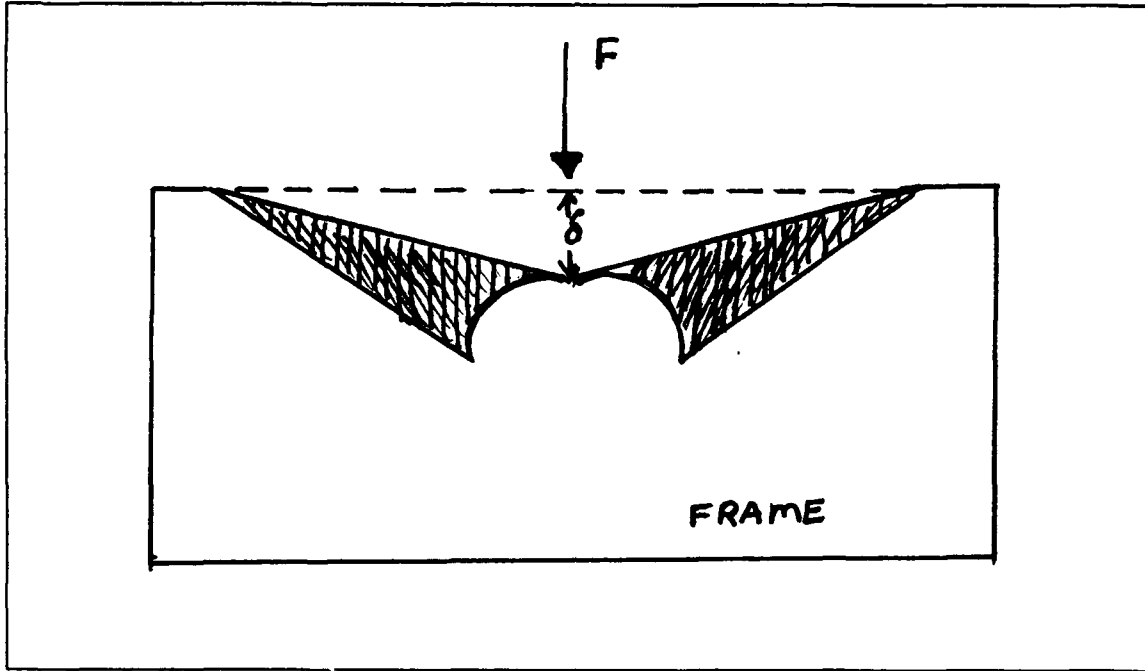


Figure 2: Transverse Frame Crushing Model

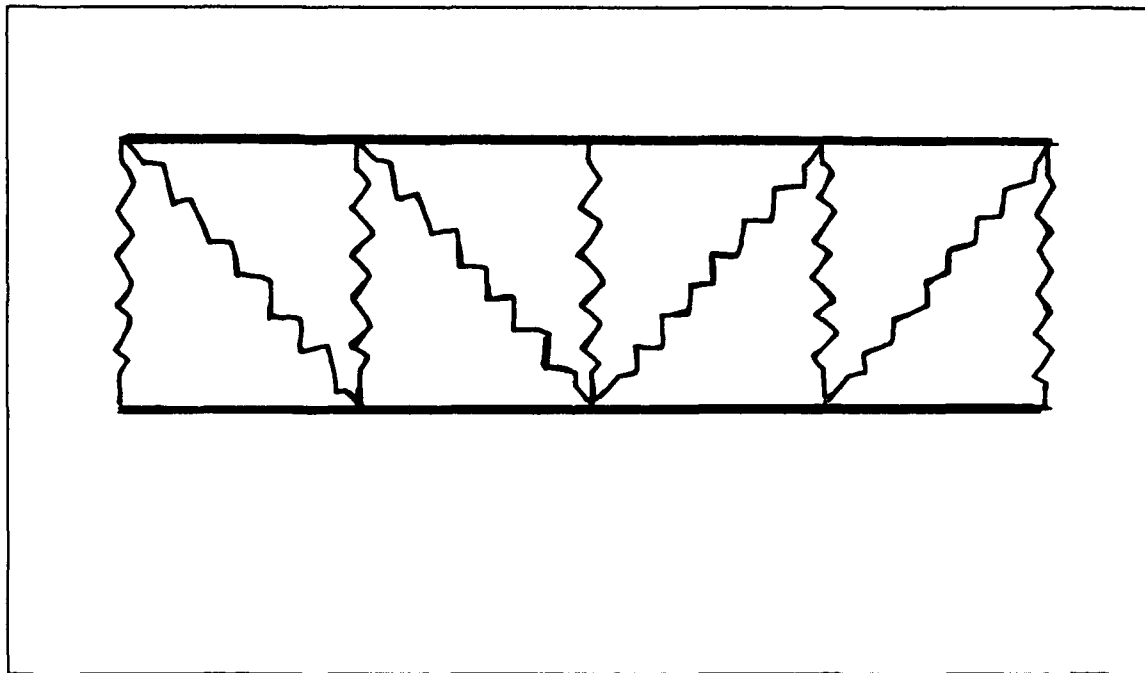


Figure 3: Spring Model of USDH

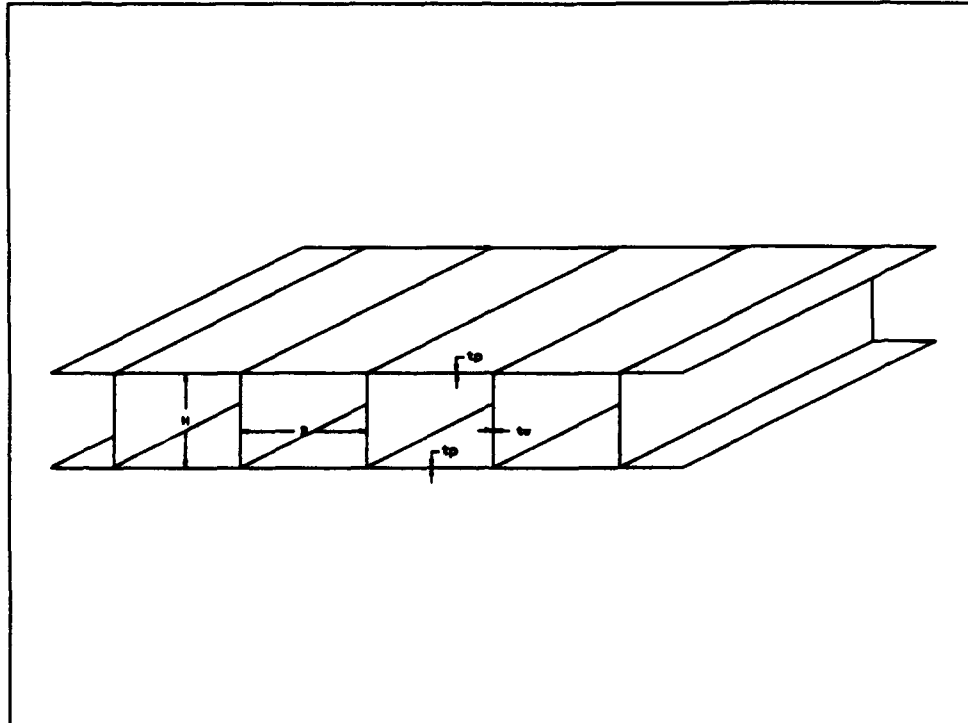


Figure 4: USDH Section

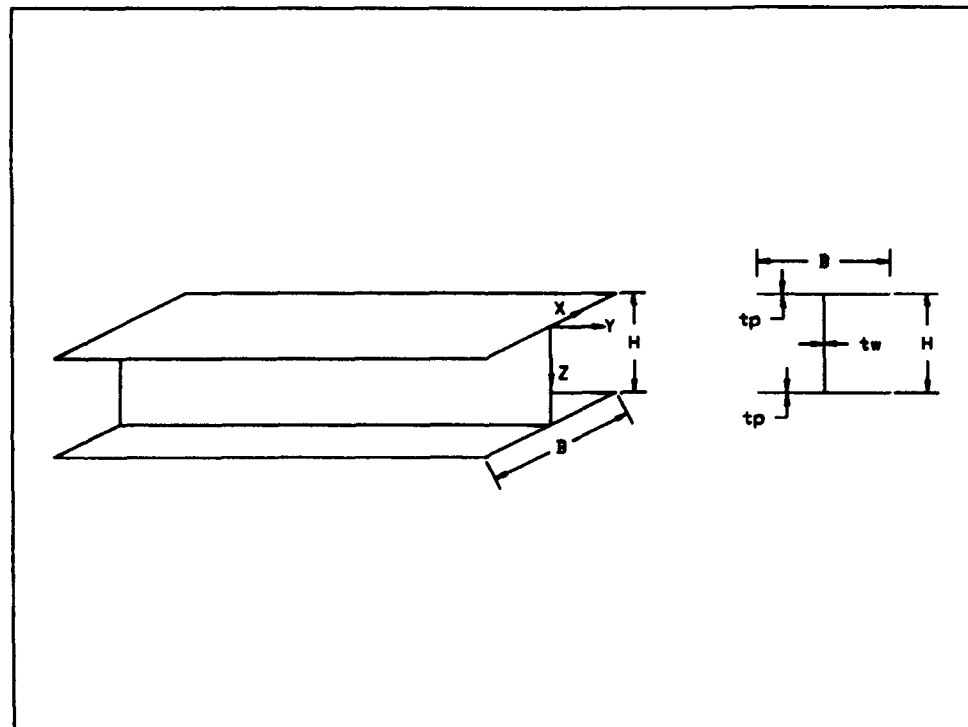


Figure 5: Structural Unit



Figure 6: Deformation of Clamped Plate

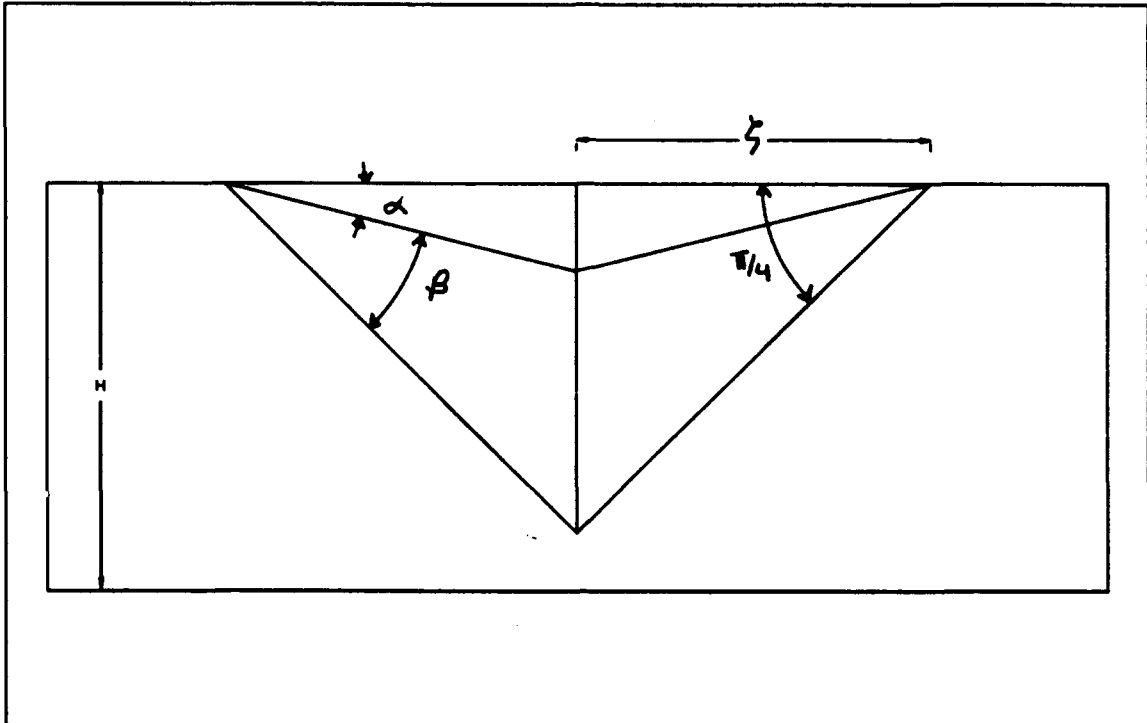


Figure 7: Local Denting Model

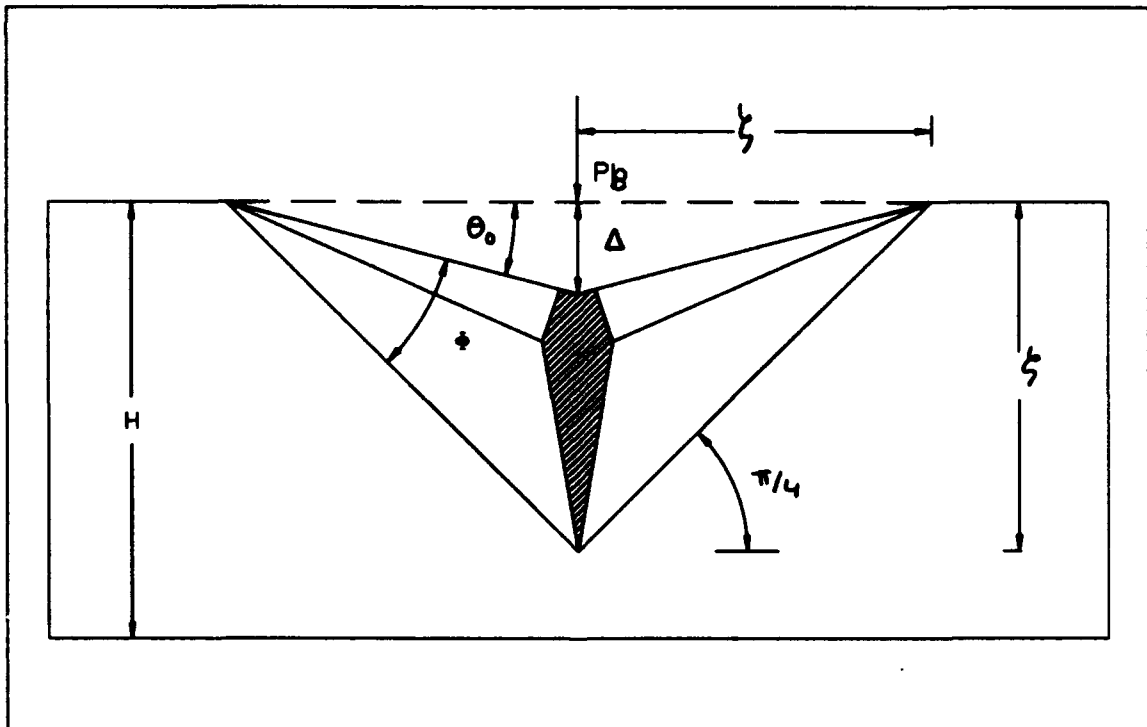


Figure 8: Deforming Web Girder

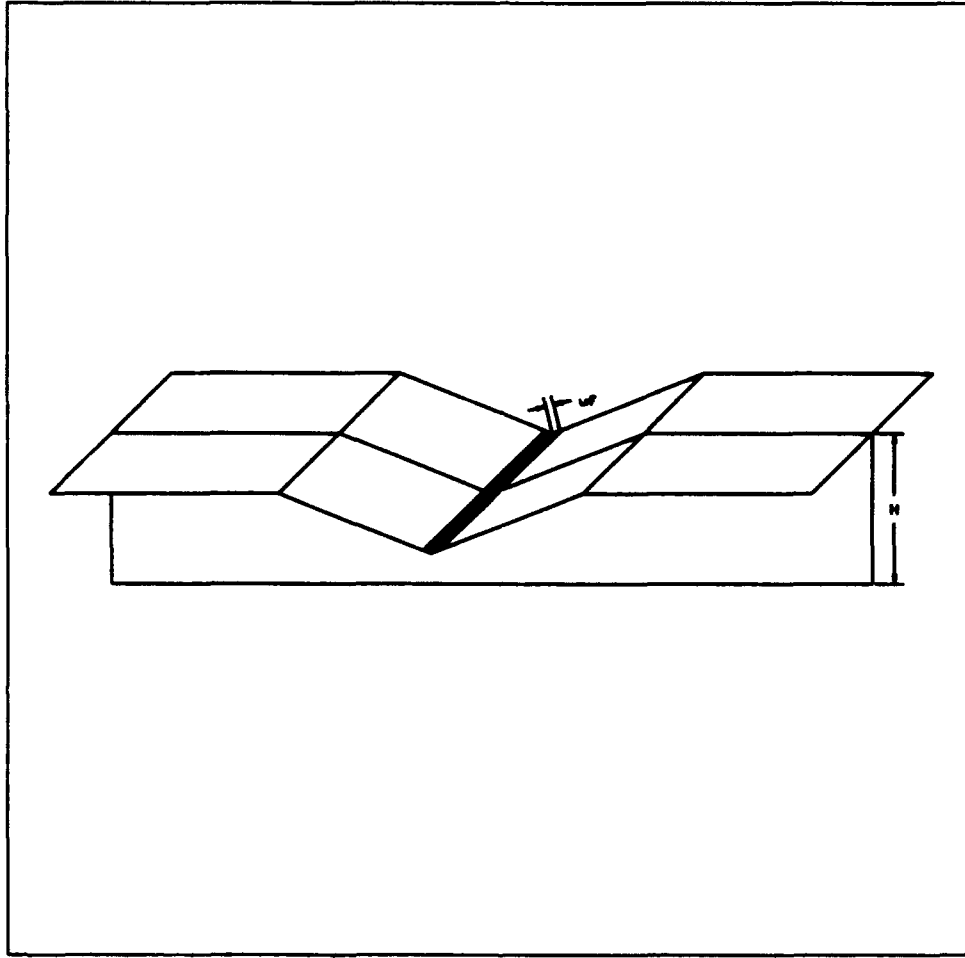


Figure 9: Deformed Flange

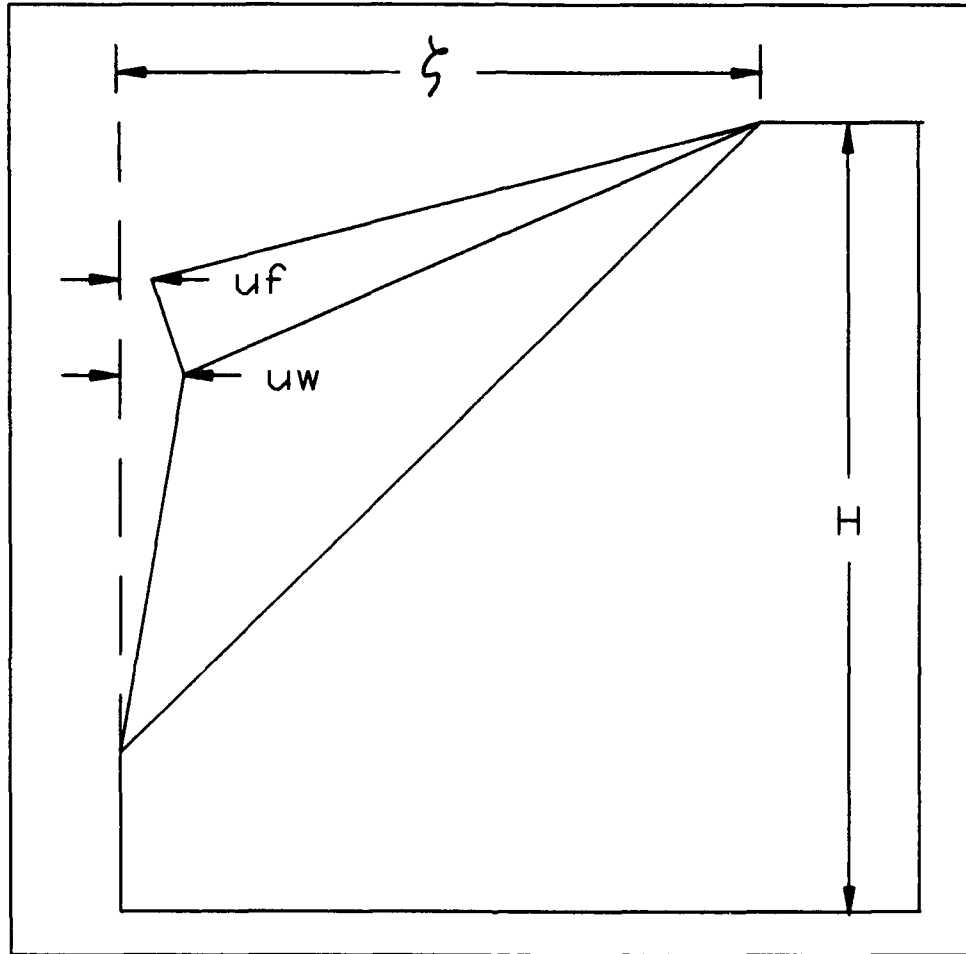


Figure 10: Stretching in Local Denting Mode

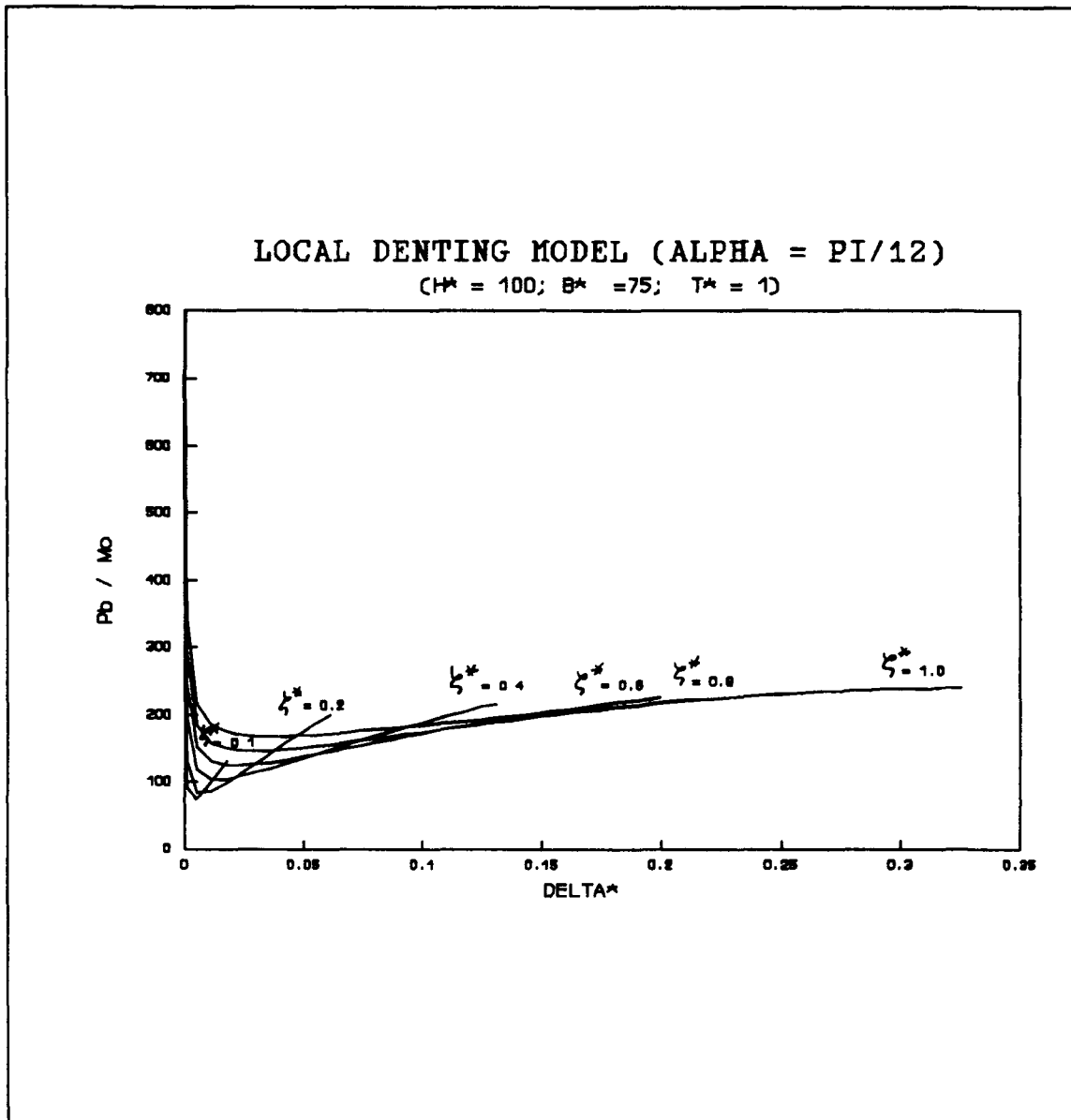


Figure 11: Local Denting Mode for  $\alpha = \pi/12$

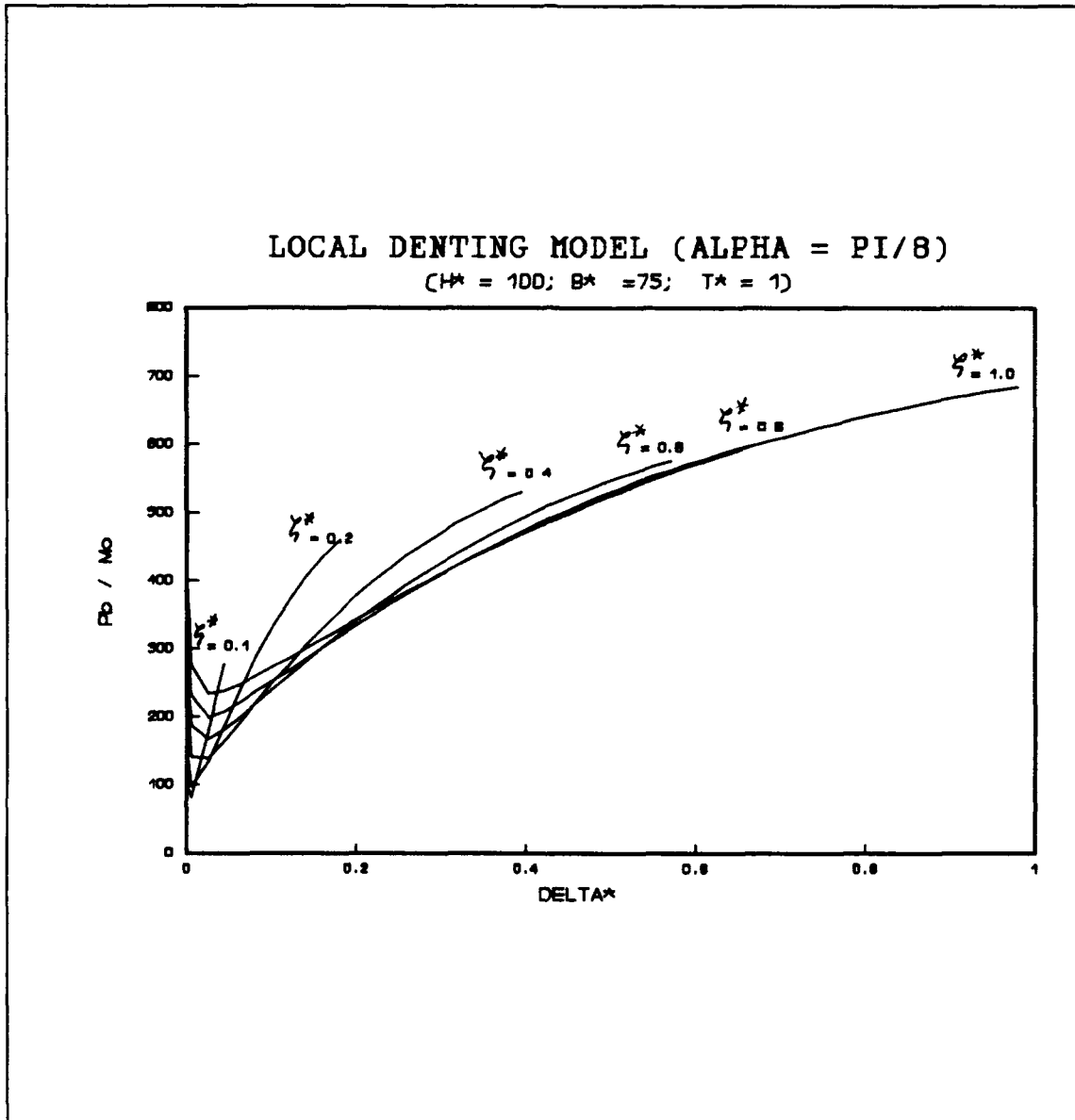


Figure 12: Local Denting Mode for  $\alpha = \pi/8$

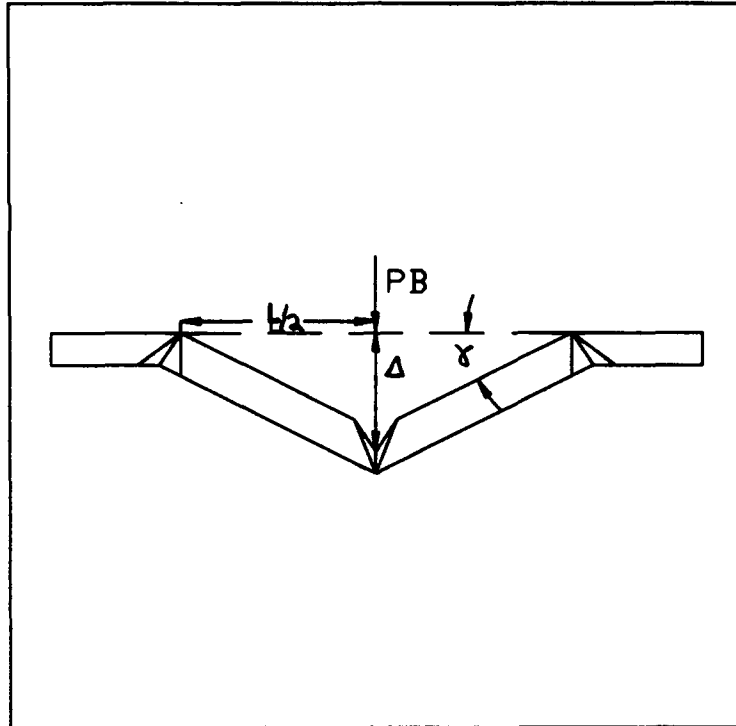


Figure 13: Three Hinge Mechanism

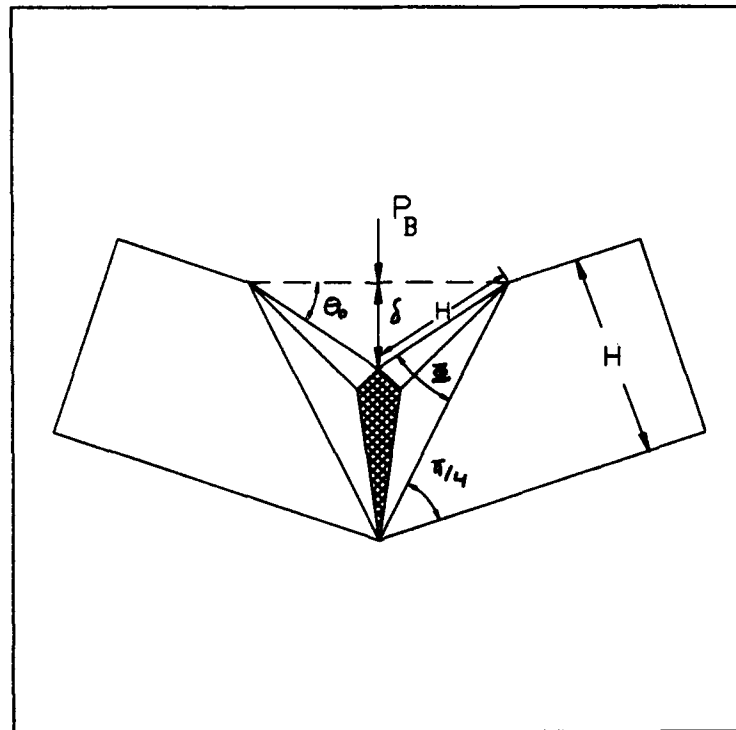


Figure 14: Hinge Point Mechanism

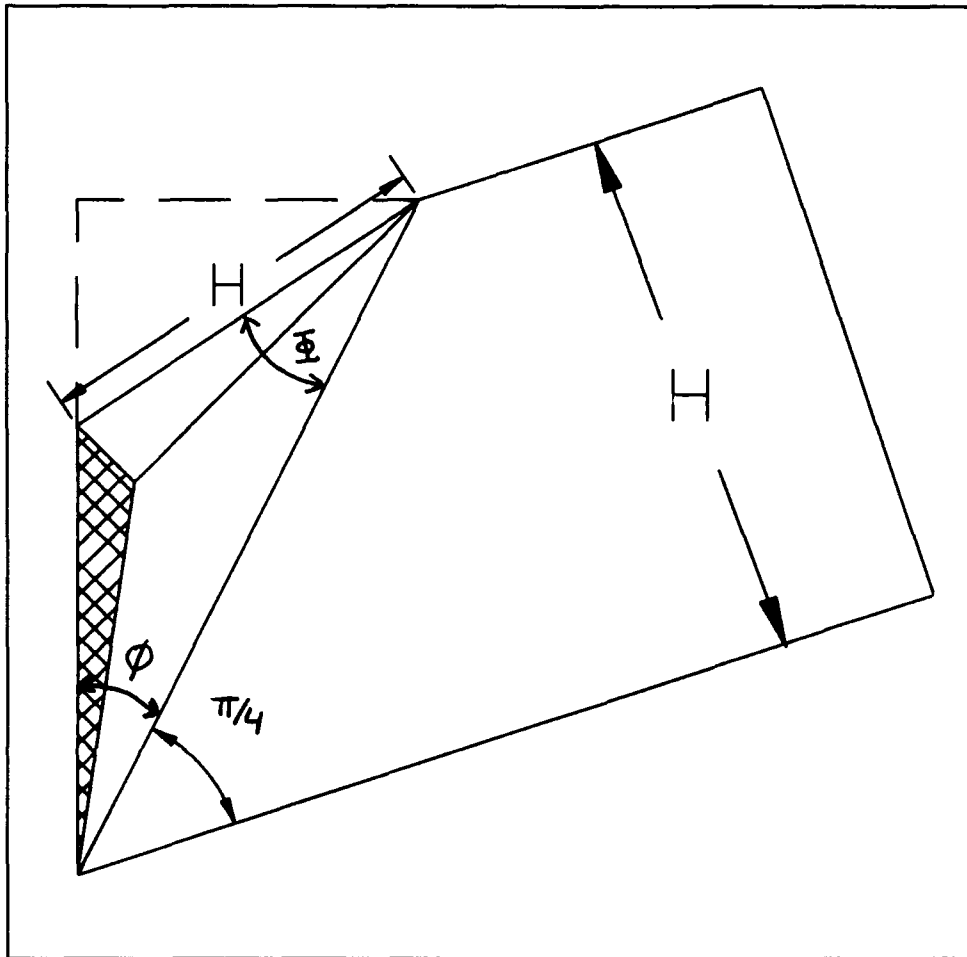


Figure 15: Stretching in Hinge Point Mechanism

# COMBINED DENTING-BENDING MODEL

( $H^*=100$ ;  $B^*=75$ ;  $T^*=1$ ;  $L^*=9$ ;  $\text{ALPHA}=\pi/12$ )

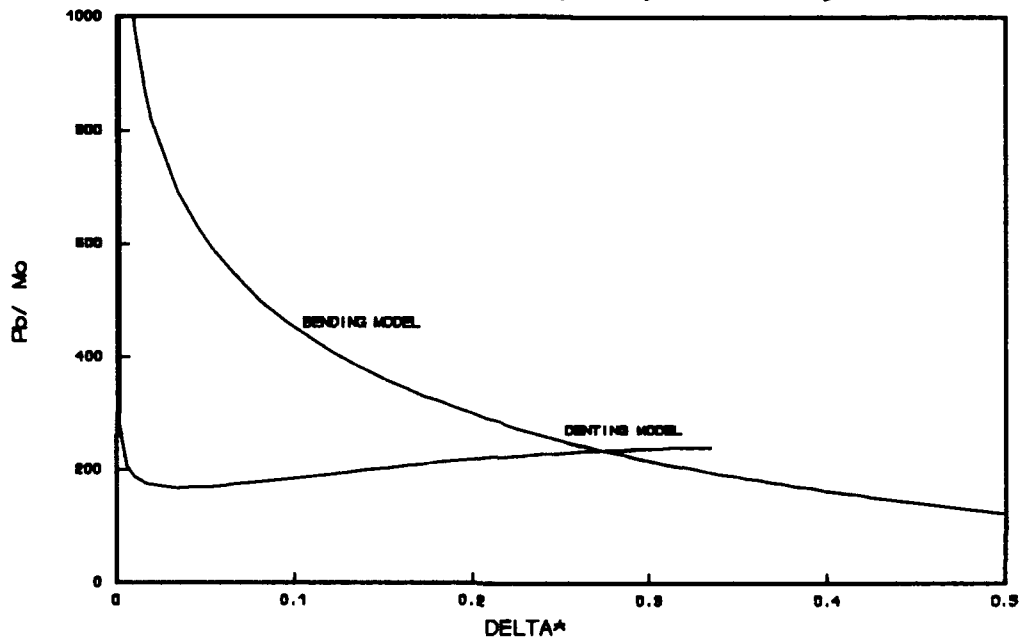


Figure 16: Global Bending Mode for  $\alpha = \pi/12$

# COMBINED DENTING-BENDING MODEL

( $H^*=100$ ;  $B^*=75$ ;  $T^*=1$ ;  $L^*=9$ ;  $\text{ALPHA}=\pi/8$ )

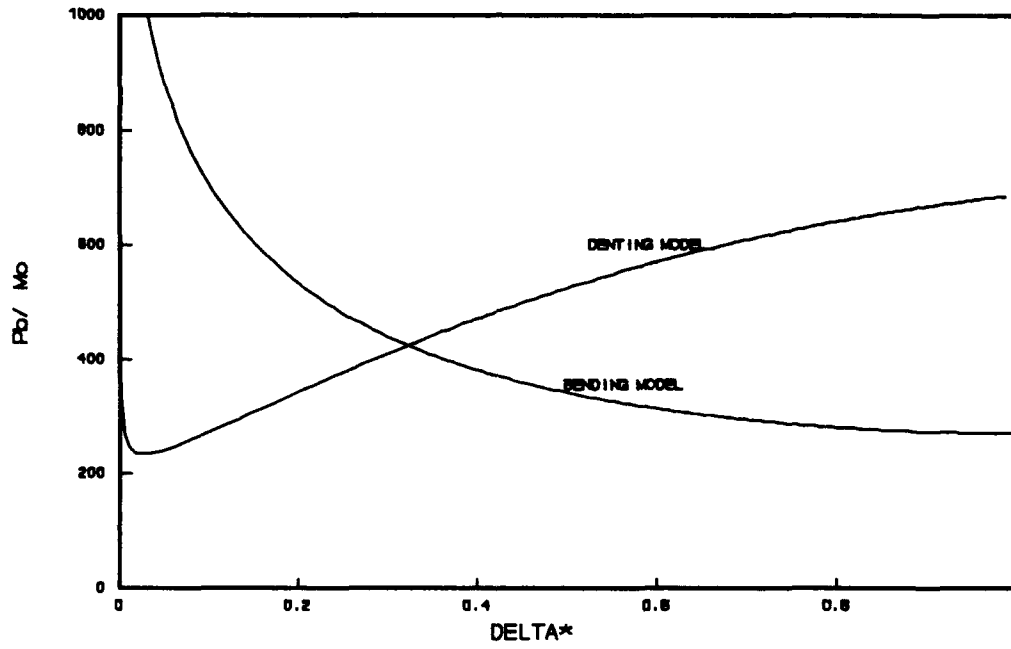


Figure 17: Global Bending Mode for  $\alpha = \pi/8$

# DENTING #1

( $H^* = 20.3$ ;  $B^* = 16.9$ ;  $T^* = 1$ ; ALPHA = P1/12)

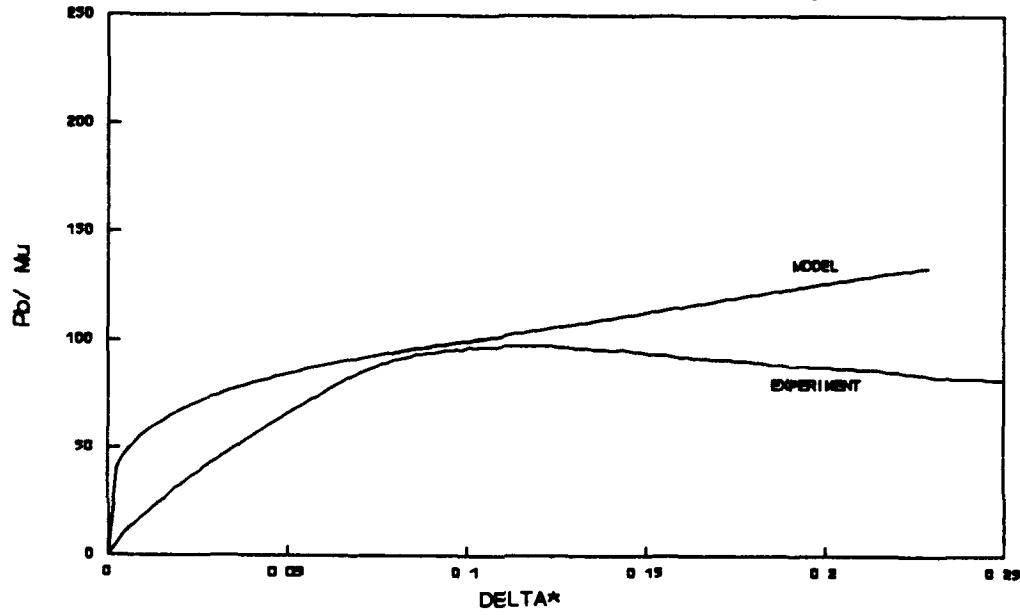


Figure 18: First Denting Experiment

# DENTING #2

( $H^* = 20.3$ ;  $B^* = 16.9$ ;  $T^* = 1$ ;  $\text{ALPHA} = \pi/12$ )

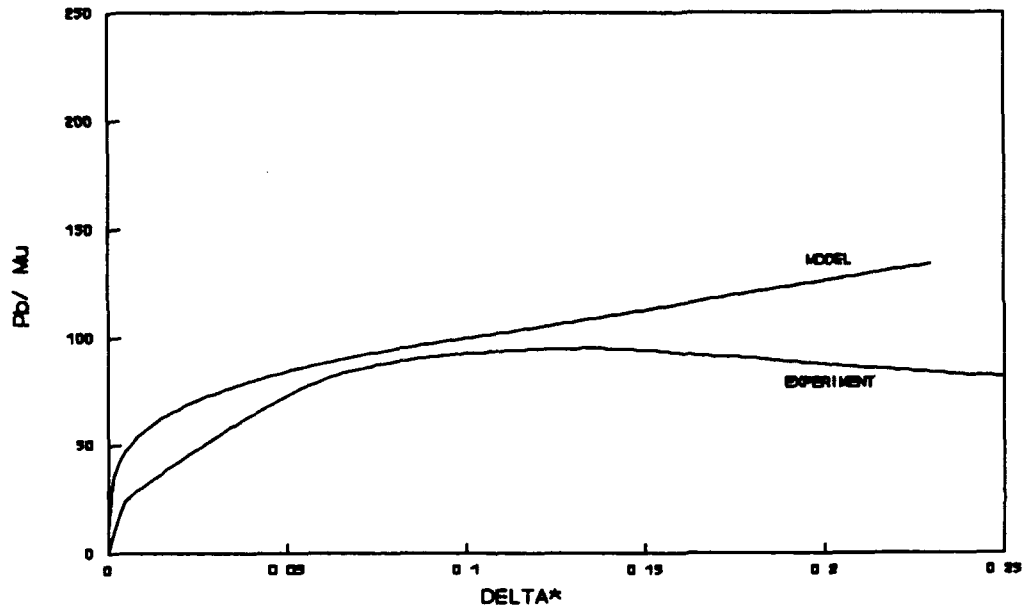
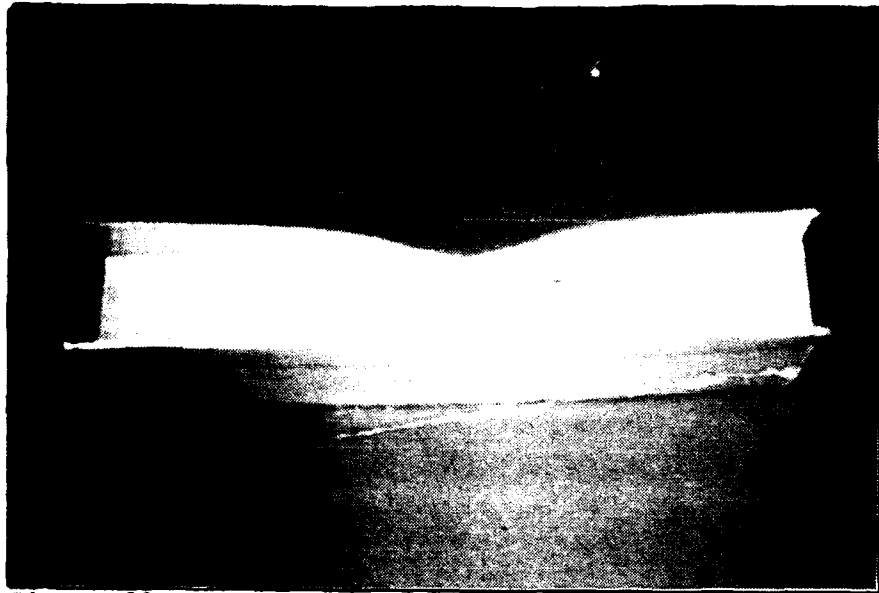


Figure 19: Second Denting Experiment



**Figure 20:** Photograph of Dented Specimen

# BENDING #1

( $H^* = 20.3$ ;  $B^* = 16.9$ ;  $T^* = 1$ ;  $L^* = 4.4$ ;  $\text{ALPHA} = \pi/8$ )

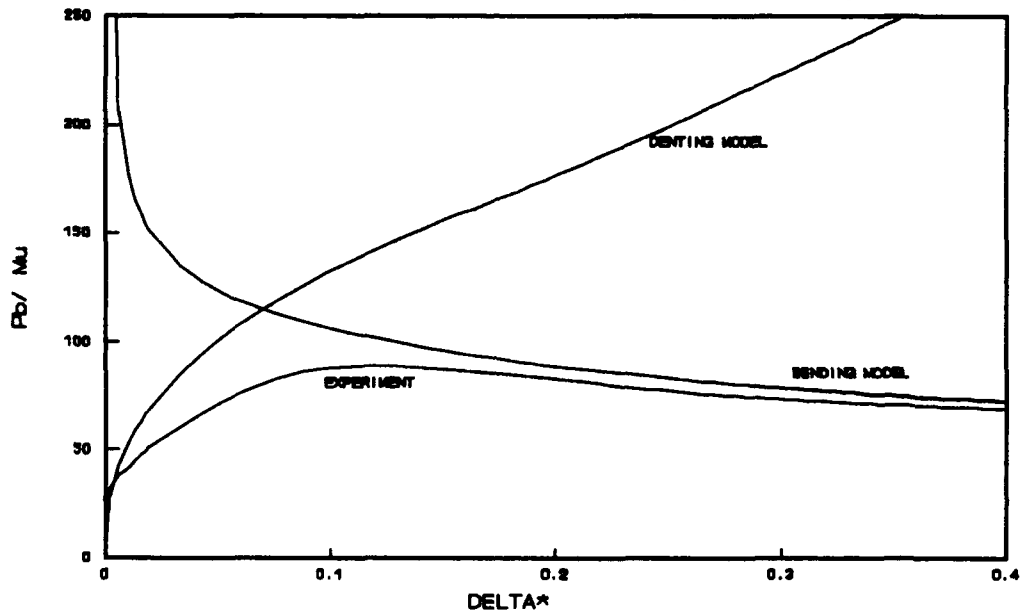


Figure 21: First Bending Experiment

# BENDING #2

( $H^*=20.3$ ;  $B^*=16.9$ ;  $T^*=1$ ;  $L^*=4.4$ ;  $\text{ALPHA}=\pi/8$ )

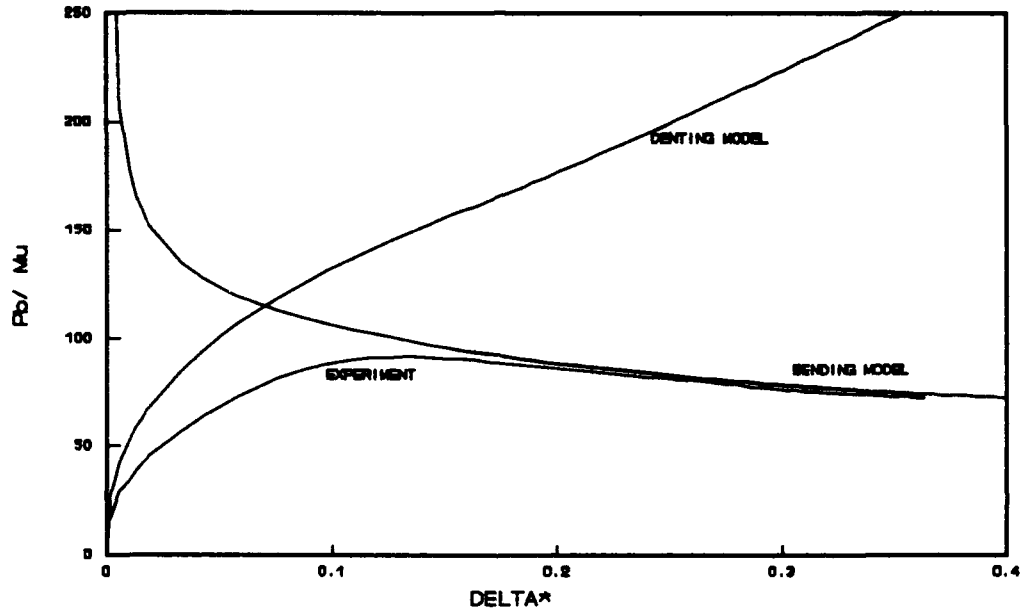
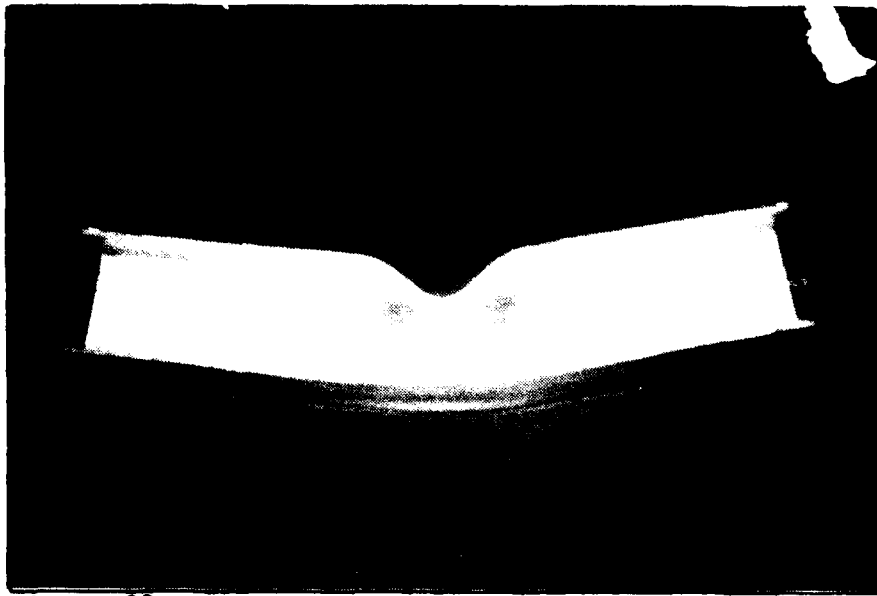
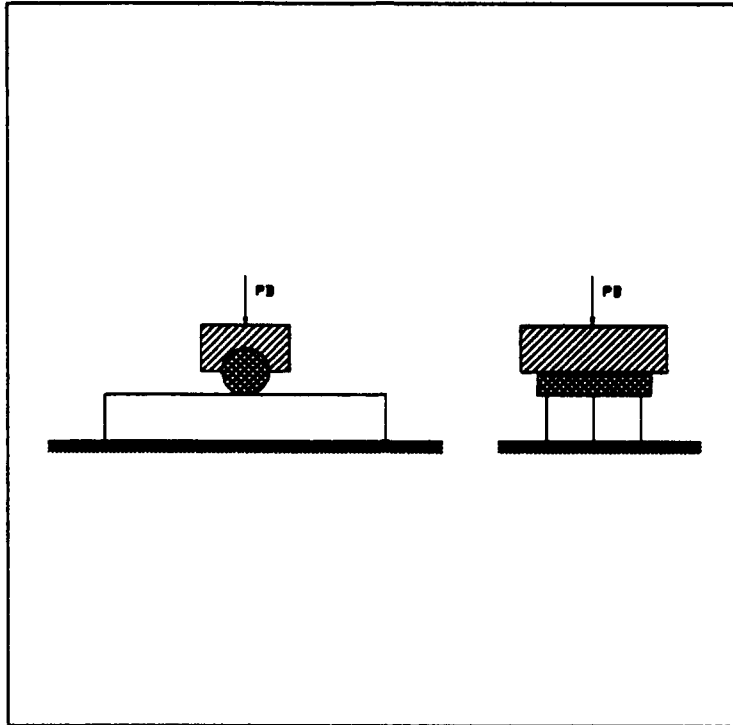


Figure 22: Second Bending Experiment



**Figure 23: Photograph of Bent Specimen**



**Figure 24: Set-up for Denting Experiments**

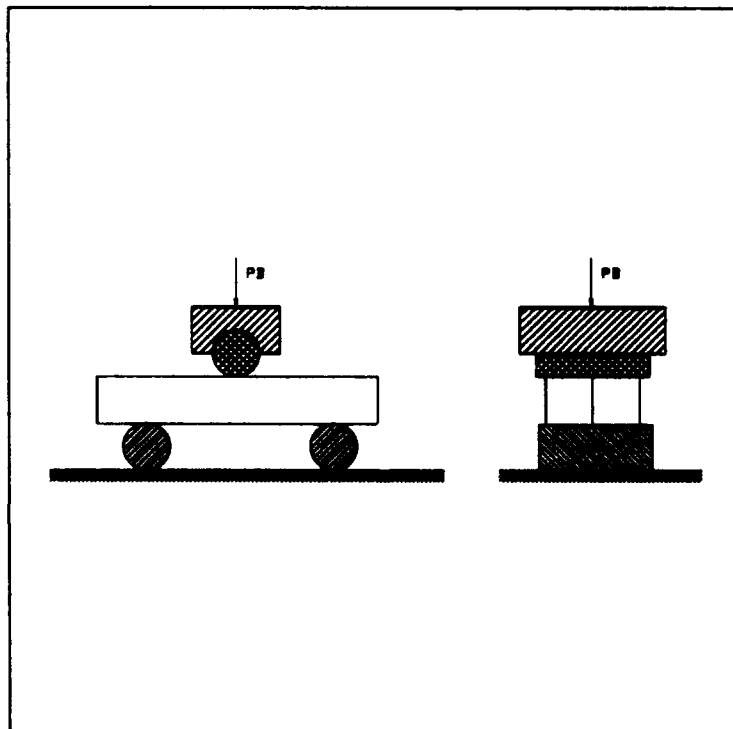


**Figure 25: Set-up for Bending Experiments**

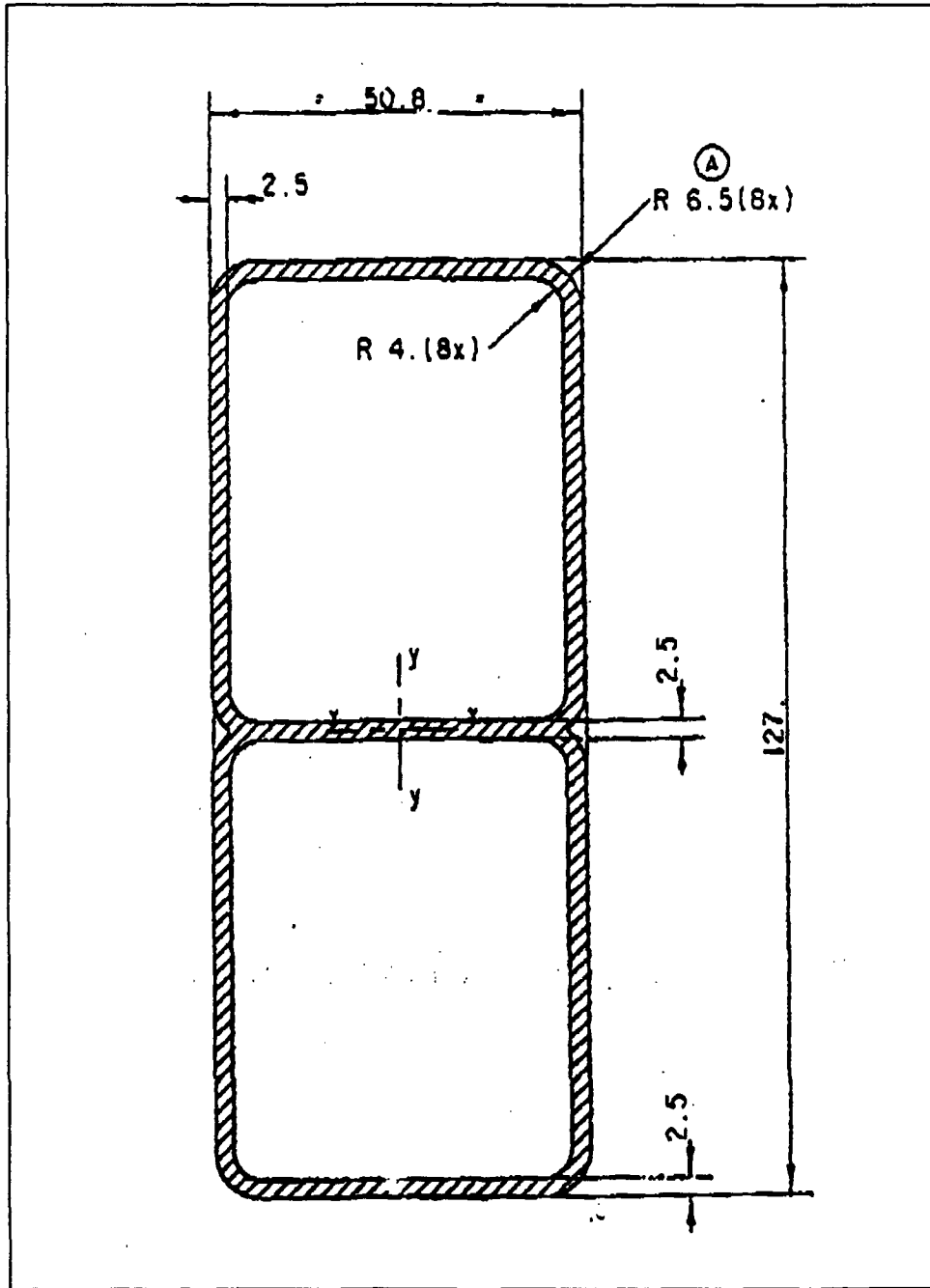
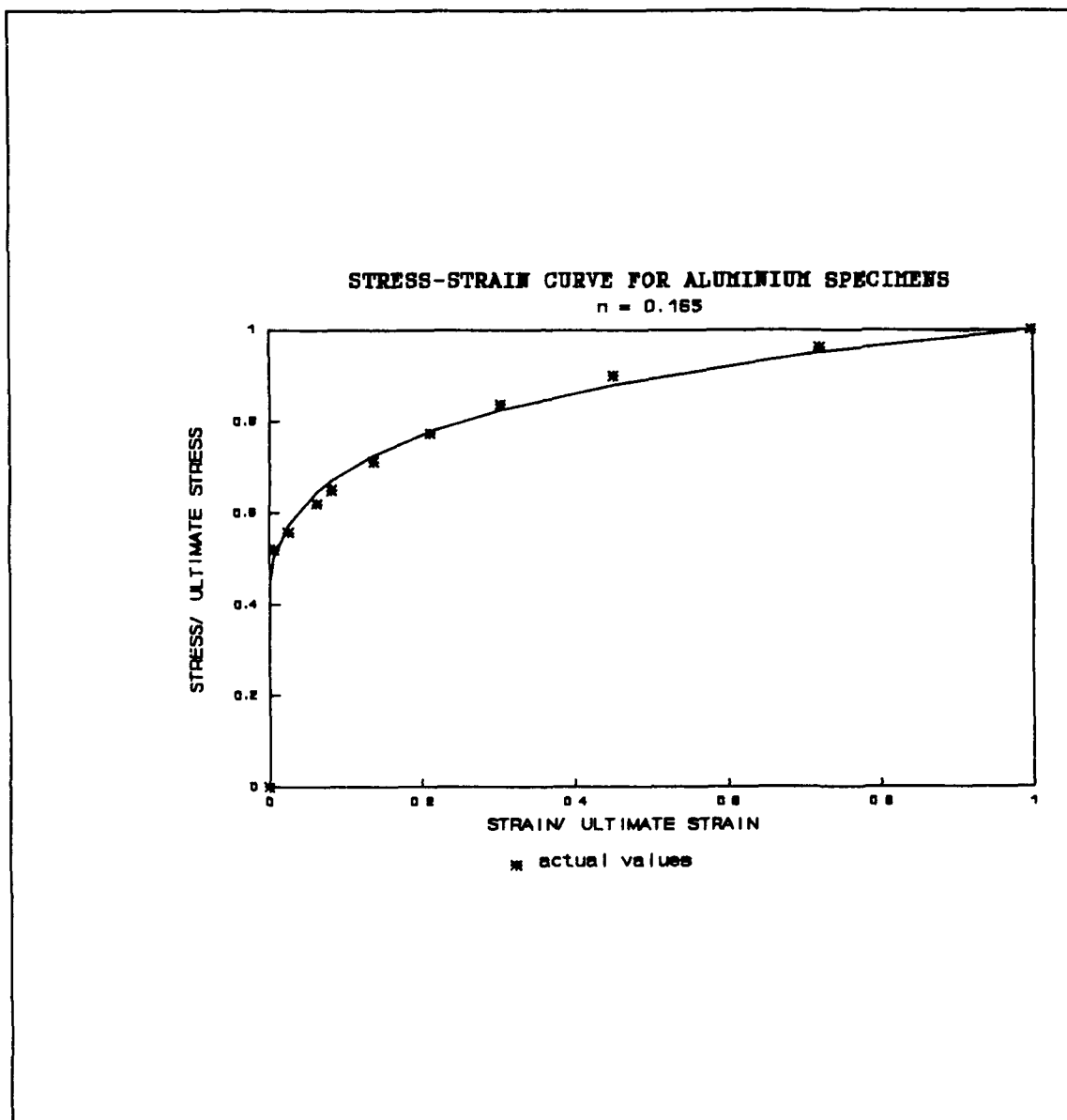


Figure 26: Specimen Cross-section



**Figure 27:** Stress-Strain Curve for Specimens